

We are IntechOpen, the world's leading publisher of Open Access books Built by scientists, for scientists

6,900

Open access books available

186,000

International authors and editors

200M

Downloads

Our authors are among the

154

Countries delivered to

TOP 1%

most cited scientists

12.2%

Contributors from top 500 universities



WEB OF SCIENCE™

Selection of our books indexed in the Book Citation Index
in Web of Science™ Core Collection (BKCI)

Interested in publishing with us?
Contact book.department@intechopen.com

Numbers displayed above are based on latest data collected.
For more information visit www.intechopen.com



Introduction

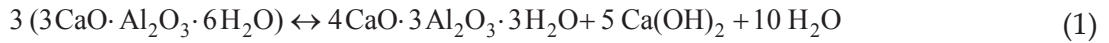
1. Discovery of strontium aluminate cements and current state of knowledge

The experimental study of the system $\text{CaO-Al}_2\text{O}_3\text{-H}_2\text{O}$ has considerable practical value not only for its direct contribution to the setting of high-alumina cements (which are composed of mainly anhydrous calcium aluminates) and Portland cements, but also for possible applications in the fields of geology, soil equilibrium, water purification, and the extraction of purified hydrated alumina from crude bauxite [1-3,12]. Unfortunately, so far the study of the system $\text{CaO-Al}_2\text{O}_3\text{-H}_2\text{O}$ has many difficulties, including [1]:

- The existence of numerous highly hydrated compounds, the determination of the degree of hydration of which is often a problem.
- Relatively low solubility of these compounds.
- The fact that most of the compounds are metastable, yet, once formed; persist over long periods of time.
- Close similarity in crystal habit and optical properties of compounds occurring as thin hexagonal (or pseudo-hexagonal) plates.
- The necessity for strict exclusion of carbon dioxide from air.

According to the results from numerous investigations of chemical reactions related to the hardening of hydraulic cements [4,12], lime and alumina in solution may combine to form isometric tri-calcium aluminate hexahydrate ($3\text{CaO}\cdot\text{Al}_2\text{O}_3\cdot 6\text{H}_2\text{O}$, C_3AH_6). This compound is isomorphic to C_3FH_6 garnet as well as grossularite garnet ($3\text{CaO}\cdot\text{Al}_2\text{O}_3\cdot 3\text{SiO}_2$, C_3AS_3) and andradite garnet ($3\text{CaO}\cdot\text{Fe}_2\text{O}_3\cdot 3\text{SiO}_2$). Complete solid solutions exist between each of these compounds and the three others. The hydrous members of the series may be termed hydrogarnets [4,5,198]. The general formula may be written as $3\text{CaO}\cdot\text{Al}_2\text{O}_3\cdot m\text{SiO}_2\cdot(6-2m)\text{H}_2\text{O}$, where m may vary from 0 to 3 [6]. Hydrogarnets crystallize in various cubic forms, of which icositetrahedra are probably the most usual at ordinary temperatures. In recent mineralogical nomenclature, the phases in the $\text{C}_3\text{AH}_6 - \text{C}_3\text{AS}_3$ series are collectively called hydrogrossular [7].

Tri-calcium aluminate hexahydrate decomposes under hydrothermal conditions at about equilibrium temperature $220 - 226^\circ\text{C}$, yielding calcium hydroxide and less basic aluminate. The equation may be written as [4,6]:



Although strontium is rather minor constituent of commonly applied cements such as Portland cement (PC) or alumina cement (AC), the strontium compounds may be formed via the reaction with silica, alumina and water. Despite the fact that the ionic radius of Sr^{2+} (1.26 and 1.44 Å for the coordination number 8 and 12, respectively [92]) is larger than that of Ca^{2+} (1.06 Å), strontium can partially replace calcium in numerous metal oxides and numerous studies concerned to Ca/Sr mixed oxides can be found in literature [8]. The existence of tri-strontium aluminate hexahydrate ($3\text{SrO} \cdot \text{Al}_2\text{O}_3 \cdot 6\text{H}_2\text{O}$) has been reported by Brandenger [9] and Maekawa [10].

Carlson [4] recognizes tri-strontium aluminate hexahydrate as the only hydrated phase formed in the system strontium – alumina – water. This phase is isomorphous with corresponding calcium compound of tri-calcium aluminate hexahydrate and the complete solid solution exists between those two phases. This is proved by the X-ray diffraction patterns, which indicate the same reflecting planes with such changes in relative intensities as might be expected for isomorphous substitutions. There is also a shift corresponding to somewhat larger unit cell of strontium compounds. The refraction index of tri-strontium aluminate hexahydrate is 1.588 [4,10].

$3\text{SrO} \cdot \text{Al}_2\text{O}_3 \cdot 6\text{H}_2\text{O}$ has higher temperature stability than $3\text{CaO} \cdot \text{Al}_2\text{O}_3 \cdot 6\text{H}_2\text{O}$, which decomposes under hydrothermal conditions according to Eq.1.1. Tri-strontium aluminate hexahydrate decomposes under hydrothermal conditions at temperatures as low as 305 °C (2 atm.) and 454 °C (420 atm.). The product of the decomposition is dependent on both the temperature and the pressure. In most cases the decomposition is accompanied by the liberation of strontium hydroxide. The lower hydrate with 1.5 molecules of water ($3\text{CaO} \cdot \text{Al}_2\text{O}_3 \cdot 1/2\text{H}_2\text{O}$, $\text{C}_3\text{AH}_{0.5}$) is probably formed. The hexagonal prism of crystalline phase $5\text{SrO} \cdot 4\text{Al}_2\text{O}_3$ was also identified as a product. It decomposes under further heating with the formation of $\text{SrO} \cdot \text{Al}_2\text{O}_3$ and $3\text{SrO} \cdot \text{Al}_2\text{O}_3$ [4].

Therefore, with SrO formally replacing CaO in calcium aluminate cement, the strontium aluminate binder belongs to the family of aluminous cements based on the system of CaO – SrO – BaO – Al_2O_3 – ZrO_2 – HfO_2 [11-14]. The differences and the similarities between the strontium – alumina and lime – alumina systems are briefly mentioned below [14]:

1. There are no compounds like Sr_5A and Sr_4A in the lime – alumina system.
2. No analog of C_{12}A_7 in the strontium – alumina system exists¹.
3. The similarities exist to some extent between Sr_3A and C_3A , SrA and CA , SrA_2 and CA_2 as well as between SrA_6 and CA_6 , although the melting behaviour and the temperature differ significantly.

¹ Phase has not own field in the equilibrium diagram of SrO- Al_2O_3 system, but the synthesis of Sr_{12}A_7 is described by Yamaguchi et al [41].

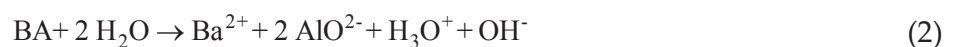
The discovery of calcium aluminates, the study of their crystal chemistry and phase equilibrium, subsequently developing the family of alumina cements and their ultimate field applications covered a span of one and half century, even though Bied received the French and the British patents for the method to produce calcium aluminate cement from bauxite and lime in a cupola furnace in 1908–1909, just about a century ago. The use of AC in basic refractories is rather limited as it leads to the formation of low-melting compounds like monticellite. In certain non-refractory applications AC shows comparatively poorer resistance to aggressive environments as well as to X-rays and gamma radiation [14].

Strontium aluminate cement can be prepared by solid-state sintering of approximately equimolar blend of SrCO_3 and Al_2O_3 at the temperature of 1500°C . The main constituent of strontium aluminate cement is mono-strontium aluminate ($\text{SrO}\cdot\text{Al}_2\text{O}_3$), but strontium hexaluminate may also be present. Strontium aluminate cement hydrates relatively slowly, yielding to strontium aluminate hexahydrate phase of the approximate composition $\text{SrO}\cdot\text{Al}_2\text{O}_3\cdot 7\text{--}10\text{H}_2\text{O}$ as the main hydration product. In later stages of hydration this phase gradually converts to $6\text{SrO}\cdot\text{Al}_2\text{O}_3\cdot 6\text{H}_2\text{O}$ and hydrous alumina. This reaction is associated with the loss of strength. The cement has the potential to be used in the production of refractory concretes [12].

Calcium and strontium aluminate cement contains Ca and Sr as the chemical elements from the second group of the periodic table (alkaline earth metals): Be (beryllium), Mg (magnesium), Ca (calcium), Sr (strontium), Ba (barium) and Ra (radium). Therefore, well-founded assumption exists to prepare similar binding system with barium, i.e. barium aluminate cement based on hydraulic properties of barium aluminate or monobarium aluminate ($\text{BaO}\cdot\text{Al}_2\text{O}_3$, BA).

Barium aluminate cement can be produced by solid-state sintering of equimolar blend of BaCO_3 (witherite) and Al_2O_3 at the temperature of $1400 - 1500^\circ\text{C}$. The sintering temperature can be reduced by the addition of suitable mineralizer such as MgO. The main constituent of such cement is barium aluminate, but small amount of tri-barium aluminate ($3\text{BaO}\cdot\text{Al}_2\text{O}_3$, B_3A) and barium hexaaluminate ($\text{BaO}\cdot 6\text{Al}_2\text{O}_3$, BA_6) is formed. At low water to cement ratios ($w/c < 0.35$), the monobarium aluminate heptahydrate ($\text{BaO}\cdot\text{Al}_2\text{O}_3\cdot 7\text{H}_2\text{O}$, BAH_7) is formed as the main hydration product. In the case that w/c ratio is higher; the tribarium aluminate hexahydrate ($3\text{BaO}\cdot\text{Al}_2\text{O}_3\cdot 6\text{H}_2\text{O}$, B_3AH_6) is formed together with hydrous alumina. The reaction of barium aluminate cement with water is fast. Whole BA hydrates completely within three days at sufficiently high water to cement ratio. The hardened cement pastes show only a small strength loss when heated to high temperatures. Barium aluminate cements can be used for the production of refractory materials and they absorb radiation effectively [12,15,19].

The initiation of hydration reactions occurs with leaching of Ba^{2+} ions and with formation of hydroxides following the reaction [14]:



Under low w/c ratio the following reactions take place:



Chaterje [14] described the pilot production process for the preparation of both BAC and SrAC cements, where raw materials in required stoichiometric proportions were cogrinded and next milled in a ball mill to the fineness of 5% residue on 212 μm sieve. The ground raw mix was treated with water and the pellets sized about 15 mm were prepared. Dried pellets were fed into a pilot rotary kiln. The sintering temperature was maintained at about 1620 $^\circ\text{C}$ and 1640 $^\circ\text{C}$ for SrAC and BAC respectively. The clinker was air quenched and ground to $300 \pm 10 \text{ m}^2 \cdot \text{kg}^{-1}$ and $280 \pm 10 \text{ m}^2 \cdot \text{kg}^{-1}$ for SrAC and BAC, respectively.

Several types of stoichiometric as well as non-stoichiometric aluminates are known. The most studied and also used aluminates of barium are the stoichiometric aluminates, such as: barium monoaluminate ($\text{BaO} \cdot \text{Al}_2\text{O}_3$, BA), tribarium monoaluminate ($3\text{BaO} \cdot \text{Al}_2\text{O}_3$, B_3A), barium tetraaluminate ($\text{BaO} \cdot 4\text{Al}_2\text{O}_3$, BA_4) and barium hexa-aluminate ($\text{BaO} \cdot 6\text{Al}_2\text{O}_3$, BA_6) [16,17,24].

All three alkali-earth monoaluminates, namely CA, SrA and BA being the primary cement-forming phases, properties are listed in Table 1. As to melting temperatures of these phases, their high-temperature stabilities sequence is as follows [14]:

$CA > SrA > BA$.

Phase	Composition[%]			Molarmass [g•mol ⁻¹]	Density [g•cm ⁻³]	Crystalsystem	Meltingtemperature/ behaviour
	Me	Al	O				
CA	25.4	34.1	40.5	158.04	2.98	Monoclinic	1605 $^\circ\text{C}$ / incongruent
SrA	42.6	26.3	31.1	205.58	3.82	Pseudo-hexagonal	1790 $^\circ\text{C}$ / congruent
BA	53.8	21.1	25.1	255.29	3.99	Cubic	1815 $^\circ\text{C}$ / congruent

Table 1. Properties of MeAl_2O_4 phases in calcium, strontium and barium aluminate cements.

Further, the traces of the liquidus curves around SrA and BA are much flatter than those around the CA phase. Thus the compositional deviations in the CA line cements are more precarious for the CA cements than the compositional shifts in BA and SrA cements [14].

2. Phase relationship in SrO – Al_2O_3 system

In this part, the phase relationships in SrO – Al_2O_3 system (Fig.1) will be discussed. The equilibrium phase diagram is useful tool for the determination of phase composition of the

Strontium oxide (strontia, strontium monoxide, SrO, S): is grayish-white colored, has elemental composition of 84.56 % Sr and 15.44 % O and cubic crystalline structure. The molar weight and the density of SrO are $103.63 \text{ g}\cdot\text{mol}^{-1}$ and $4.70 \text{ g}\cdot\text{cm}^{-3}$, respectively. It melts at the temperature of $2430 \text{ }^\circ\text{C}$ and vaporizes above $3000 \text{ }^\circ\text{C}$. It reacts with water to strontium hydroxide ($\text{Sr}(\text{OH})_2$) evolving heat. Strontium oxide can be prepared by thermal decomposition of strontium carbonate, hydroxide, or nitrate [91]:



SrO is miscible with fused caustic potash, is slightly soluble in alcohol and insoluble in acetone and ether [91]. The methods used for industrial production of strontium carbonate as the intermediate for the preparation of other compounds of strontium is described in Chapter 2.1.1.

Tetrastrontium aluminate ($\text{Sr}_4\text{Al}_2\text{O}_7$, $4\text{SrO}\cdot\text{Al}_2\text{O}_3$, Sr_4A): this phase is stable only within the temperature range from 1125 to $1630 \text{ }^\circ\text{C}$. It decomposes into mixture of tri-strontium aluminate and free strontium oxide if the temperature is lower than $1125 \text{ }^\circ\text{C}$, peritectic melting takes place at the temperature of $1630 \text{ }^\circ\text{C}$. In the temperature of $1320 \text{ }^\circ\text{C}$ the high temperature modification of α -phase is transformed into low temperature β -phase. As can be read from the phase diagram in Fig.1, the low temperature modification of tetra-strontium aluminate forms solid solution with tri-strontium aluminate [14].

Tristrontium aluminate ($\text{Sr}_3\text{Al}_2\text{O}_6$, $3\text{SrO}\cdot\text{Al}_2\text{O}_3$, Sr_3A): has cubic “*stuffed-tridimite*” structure with the space group $Pa\bar{3}$ based on $(\text{AlO}_3)_6$ rings. The noteworthy feature of this structure is the puckered six-membered tetrahedral AlO_4 rings. There is a front layer and a back layer in this structure, each running in parallel to the other. This structure is typical for strontium aluminates where either tetrahedral AlO_4 or octahedral AlO_6 groups are present (or sometimes both). The lattice parameters are $a=15.8556 \text{ \AA}$, $V=3986.3 \text{ \AA}^3$, $Z=24$ [19]. The structure of strontium aluminate is shown in Fig.2(a).

Strontium aluminate (SrAl_2O_4 , $\text{SrO}\cdot\text{Al}_2\text{O}_3$, SrA): white color, melts congruently at the temperature of $1790 \text{ }^\circ\text{C}$. The spinel type (AB_2O_4) compound has monoclinic structure that belongs to the $\text{P}2_1$ or $\text{P}2_1/m$ space group with unit cell parameters $a=5.1497 \text{ \AA}$, $b=8.836 \text{ \AA}$, $c=8.442 \text{ \AA}$, $\beta=93.43^\circ$ and contains four formula per cell ($Z=4$). SrAl_2O_4 structure is derived from “*stuffed tridimite structure*”, where all Si^{4+} cations are replaced by Al^{3+} and the charge compensating cations Sr^{2+} occupy the large open channels in the framework². Strontium aluminate is an

² Analogically to the structure of CaAl_2O_4 and BaAl_2O_4 that belong to the family of tridymite stuffed derivatives of MAl_2O_4 , where $\text{M} = \text{Ca}, \text{Sr}, \text{Ba}$. This structure is also typical for compounds such as BaNSiO_4 ($\text{N} = \text{Co}, \text{Mg}$ and Zn) and $(\text{Na}, \text{K})\text{ZXGeO}_4$ ($\text{Z} = \text{Al}$ and Ga and $\text{X} = \text{Ge}$ and Si [22]). The structure is similar to zeolites, but differs in the orientation of corner-connected tetrahedral units in the way that some of 6-membered rings convert to 4- and 8-membered rings [23].

indirect-band-gap oxide and its band gap was estimated to ~ 6.9 eV [19-23]. The structure of strontium aluminate is shown in Fig.2(b). The high temperature hexagonal polymorph is of $P6_3$ space group with the cell parameters: $a=8.926$ Å, $c=8.4985$ Å, $\gamma=120^\circ$ and $Z=6$ [24].

Strontium dialuminate (SrAl_4O_7 , $\text{SrO}\cdot 2\text{Al}_2\text{O}_3$, SrA_2): has two polymorphs, α - SrA_2 is stable at normal pressures, while high pressure form of β - SrA_2 can be prepared only at high pressure and temperature. The crystals of β - SrA_2 are orthorhombic with the space group $Cmma$, $a=8.085$ Å, $b=11.845$ Å, $c=4.407$, $Z=4$ and calculated density of 4.84 g cm^{-3} . The lattice consists of three-dimensional (Al_4O_7) network of AlO_6 octahedra (length bond from 1.795 to 1.968 Å) and AlO_4 tetrahedra (length bond from 1.449 to 1.537 Å). The structure has certain similarities to the structure of tetra-strontium aluminate. Each atom of Sr is surrounded by 10 O atoms with the distances ranging from 2.503 to 2.664 Å [19,25]. Monoclinic α - SrA_2 has the space group $C12/c1$ with the lattice parameters $a=13.0389$ Å, $b=9.0113$ Å, $c=5.5358$ Å, $\beta=106.12^\circ$ and $Z=4$ [26].

Strontium hexaaluminate ($\text{SrAl}_{12}\text{O}_{19}$, $\text{SrO}\cdot 6\text{Al}_2\text{O}_3$, SrA_6): this phase has hexagonal magnetoplumbite structure³ with space group $P6/mmc$. These compounds have a layer structure composed of spinel blocks and conduction layers which are stacked alternately (Fig.2(c)). There are five distinct Al^{3+} sites in the lattice: one tetrahedral (Al(IV) , AlO_4 with C_{3v} site symmetry) one trigonal bipyramidal (Al(V) , AlO_5 with C_{3v} site symmetry) and three octahedral (Al(VI) , AlO_6). The octahedral sites are of different symmetry: regular octahedron (D_{3d} , Al(VI)-1), antiprism (C_{3v} , Al(VI)-2) and distorted octahedron (C_s , Al(VI)-3). The Al(V) sites are present only in so called “central atom model” (residual factor 0.0340) while half occupied site of distorted tetrahedron (Al(IV)-d of C_{3v} site symmetry) results from later “split atom model” (residual factor 0.0331). The unit cell is composed of spinel-structured slabs containing Al^{3+} cations separated by mirror planes ($2b^4$ site in the central atom model and $4e$ with half occupancy in the split atom model) which contain Sr^{2+} and three oxygen ions per unit cell. The band gap of strontium aluminate is about 7.6 eV [19,27,28,29,30].

The unit cell parameters of $\text{SrAl}_{12}\text{O}_{19}$ hexagonal cell are: $a=5.562$, $c=21.972$ Å and $Z=2$ [31,32]. Small divalent cations Mg^{2+} can be incorporated in the spinel block with replacing trivalent Al^{3+} ions and the difference of their ionic valences causes the defects in the structure or sometimes the modification of the structure [33]:

- Mg replaces Al in the Al-spinel block, inducing a valence deficiency. A charge compensation with positively charged conduction layer is required.
- Spinel unit ($\text{Mg}_2\text{Al}_4\text{O}_8$) will be inserted in the Al-spinel block.
- Al^{3+} ions in octahedral sites should be replaced by Fe^{3+} [34,35], Cr^{3+} [36], Co^{3+} [36,37], Mn^{2+} [38] and rare earth elements ions such as Y^{3+} [39] or Ga^{3+} [40].

³ MP-type alkaline earth (AE) aluminum oxide ($\text{AEAl}_{12}\text{O}_{19}$). These compounds belong to the same space group as β -alumina (Chapter 4.2).

⁴ Wyckoff position denotes the point belonging to a set of points for which the site symmetry groups are conjugate subgroups of the space group.

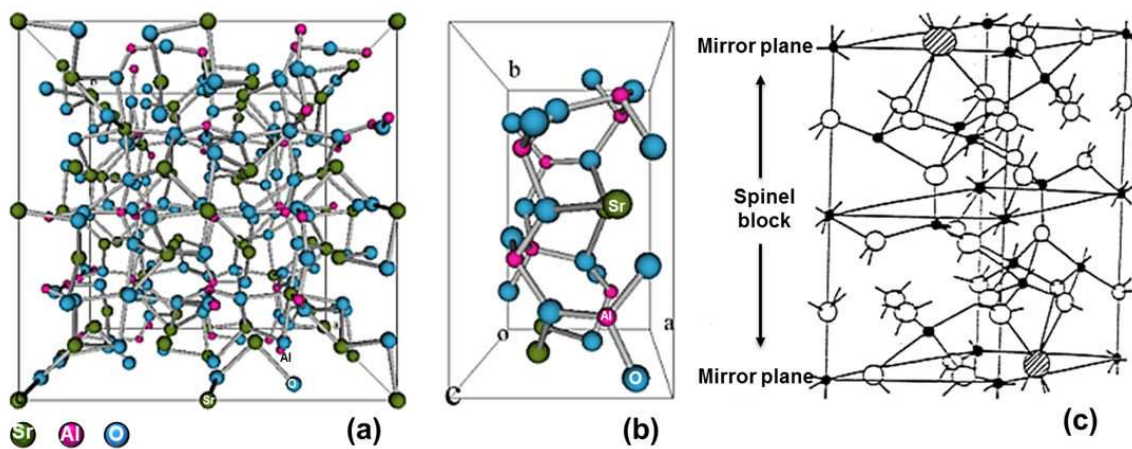


Figure 2. Structure of tristrontium aluminate (a) and strontium aluminate (b), schematic drawing of the structure of magnetoplumbite compounds (c) according to [24], where large shaded circles represent large cations (Na⁺, K⁺, Sr²⁺ ...), white and black circles represent O²⁻ and Al³⁺, respectively.

Aluminium oxide (Al₂O₃, A): belongs to the $R\bar{3}c$ space group and forms hexagonal crystal (in the only thermodynamically stable crystallographic modification of corundum, α -Al₂O₃) with the lattice cell parameters ($a=4.754 \text{ \AA}$ and $c=12.99 \text{ \AA}$). O²⁻ ions are arranged in close hexagonal arrangement, with cations Al³⁺ occupying two-thirds of the octahedral interstitial positions. Corundum has the density of $3.97 \text{ g}\cdot\text{cm}^{-3}$ and the elemental composition of 52.91% Al and 47.08% O.

The molar weight of aluminium oxide is $101.96 \text{ g}\cdot\text{mol}^{-1}$. Al₂O₃ is available or prepared in several forms for various commercial applications. Some of these are α -alumina (corundum), activated aluminas (such as, γ -alumina, η -alumina and ρ -alumina), hydrated aluminas including aluminum oxide monohydrate, Al₂O₃•H₂O and aluminum oxide trihydrate, Al₂O₃•3H₂O (natural gibbsite) and acidic, neutral and basic aluminas (no definite chemical compositions, they are prepared by the addition of various amounts of water to activated aluminas). Alumina exhibits amphoteric behaviour [91,424]. The properties and the methods of industrial production of Al₂O₃ are described in Chapter 2.1.2.

Other phases found and described within the SrO – Al₂O₃ oxide system, which aren't plotted in the equilibrium phase diagram (Fig.1) are:

- **Sr₁₂Al₁₄O₃₃ (12SrO·7Al₂O₃):** has cubic structure of space group I43d and following cell parameters: $a=12.325 \text{ \AA}$ and $Z=2$ [41].
- **Sr₁₀Al₆O₁₉ (10SrO·3Al₂O₃):** has monoclinic structure (space group C12/c1, $a=35.5823 \text{ \AA}$, $b=7.8460 \text{ \AA}$, $c=15.7485 \text{ \AA}$, $\beta=103.68^\circ$ and $Z=8$, Fig.3), which belongs to the group of oligoaluminates, where the prominent structural features are [Al₆O₁₉] – groups. The arrangement of tetrahedra within hexamers is not linear but highly puckered. In detail, the geometry can be characterized as open five-membered tetrahedral rings with one additionally attached sixth tetrahedron. The Al-O bond distances in Sr₆Al₁₀O₁₉ range between 1.73 and 1.81 \AA [42]. Sr₆Al₁₀O₁₉ is isotopic with strontium gallate α -Sr₁₀Ga₆O₁₉ [43].

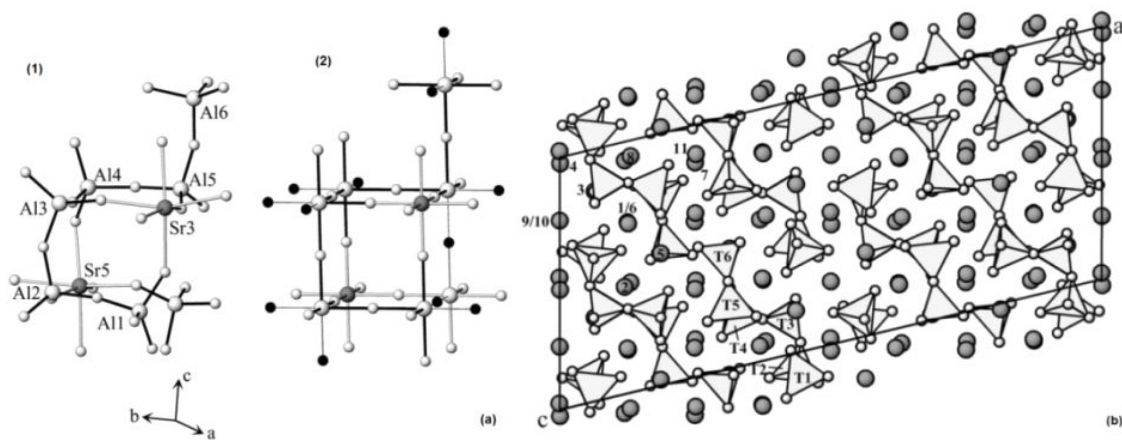


Figure 3. Single $[Al_6O_{19}]$ hexamer in the structure of $Sr_{10}Al_6O_{19}$ with two linking tetrahedra (1) and the arrangement of cations, anions and vacancies in the corresponding idealized unit of perovskite (2) containing atoms of Sr (big dark spheres) and Al (light gray spheres), oxygen ligands (small gray spheres) and vacancies (small dark spheres). Al-O bonds within $[Al_6O_{19}]$ hexamer are represented by dark rod (a). The structure of $Sr_{10}Al_6O_{19}$, projection is parallel with $[010]$ (b). Big gray spheres corresponding to Sr cations and tetrahedra (T) belonging to one of single $[Al_6O_{19}]$ hexamers are marked [42].

- **$Sr_7Al_{12}O_{25}$ ($7SrO \cdot 6Al_2O_3$):** is trigonal phase with the space group $P3$ and following cell parameters $a=11.91 \text{ \AA}$, $\gamma=120^\circ$ and $Z=3$ [44].
- **$Sr_4Al_{14}O_{25}$ ($4SrO \cdot 7Al_2O_3$):** is orthorhombic phase of $Pnna$ space group with following cell parameters: $a=24.7451 \text{ \AA}$, $b=8.4735 \text{ \AA}$, $c=4.8808 \text{ \AA}$ and $Z=2$ [45].
- **$Sr_2Al_6O_{11}$ ($2SrO \cdot 3Al_2O_3$):** is orthorhombic phase of $Pnmm$ space group with following cell parameters: $a=21.914 \text{ \AA}$, $b=4.884 \text{ \AA}$, $c=8.4039 \text{ \AA}$ and $Z=4$ [46].

2.1. Application of Gibbs phase law on the phase diagram

The Gibbs phase rule [47] enables to calculate the number of degrees of freedom of the system. The most general and well known formulation is:

$$v = s - f + 2 - C \quad (9)$$

where v , s and f denote the number of degrees of freedom, species (constituents) and phases, respectively. Number "two" represents the temperature and pressure. The value of parameter C is derived from other restriction conditions in given thermodynamic system, for example from the number of independent chemical reactions (Gibbs stoichiometric law, Chapter 1.4), from the Dalton law, from the principle of electroneutrality, etc.).

The Gibbs phase law can be derived from the following consideration which includes the system formed from s species and f phases. There are certain minimal numbers of parameters which are necessary to describe the state of this system ($f(s-1)+2$):

$$\begin{aligned}
 x_s^1 &= 1 - \sum_{j=1}^{s-1} x_j^1 \\
 &\vdots \\
 x_s^f &= 1 - \sum_{j=1}^{s-1} x_j^f
 \end{aligned} \tag{10}$$

There is also certain minimal number of parameters which are necessary to describe the equilibrium in the system. The equilibrium is defined as the equivalence of chemical potential of s components across $f-1$ phases, i.e. $s(f-1)$ variables.

$$\begin{aligned}
 \mu_1^1 &= \mu_1^2 = \dots = \mu_1^{f-1} \\
 \mu_2^1 &= \mu_2^2 = \dots = \mu_2^{f-1} \\
 &\vdots \\
 \mu_s^1 &= \mu_s^2 = \dots = \mu_s^{f-1}
 \end{aligned} \tag{11}$$

For example, if we consider a system that consists of two components and three phases (e.g. some of eutectic points or the formation of peritectic melt in Fig.1), the condition can be explained as follows: if $\mu_{11}=\mu_{12}$ and $\mu_{12}=\mu_{13}$ then $\mu_{11}=\mu_{13}$. Therefore, only $2 \times (3-1)=4$ terms are necessary for the description of equilibrium.

The Gibbs phase law is a simple difference between the number of parameters defining the state and the equilibrium in the system:

$$v = f(s-1) + 2 - s(f-1) = fs - f + 2 - fs + s \tag{12}$$

$$v = s - f + 2 \tag{13}$$

In the case of isobaric type $[p]$ of phase diagram in Fig.1 without other restricting condition ($C=0$) it is possible to write:

$$v = s - f + 1 \tag{14}$$

2.2. Phase diagram and lever law

The equilibrium phase diagram or isobaric equilibrium phase diagram is a useful tool, which enables to predict the system behaviour during the thermal treatment. It is possible to estimate:

- Final phase composition of material;
- Field of stability (temperature and composition) of formed phases;

- Formation and decomposition of solid solutions;
- Melting temperature;
- Composition and temperature of invariant points (eutectic and peritectic points);
- Behaviour during melting (congruent or incongruent);
- Immiscibility gap in melt;
- Behaviour during crystallization;
- Ratio of formed phases.

Moreover is possible to predict the structure of cooled product (for example grain of precipitate dispersed in matrix of solidified eutectic melt) or to calculate melting enthalpy from the liquids line of diagram (described in Chapter 2.3).

It should be pointed out, that the equilibrium phase composition is not often established during industrial production of materials, especially during fast firing process of ceramics. Moreover metastable phases exhibit higher reactivity, therefore are often prepared purposely. For example, fast cooling of clinker of ordinary Portland cement (OPC) is applied in order to prevent it from the decomposition of tricalcium silicate ($C_3S, 3CaO \cdot SiO_2$) into dicalcium silicate and free lime (C, CaO), as well as to keep the formed dicalcium silicate ($C_2S, 2CaO \cdot SiO_2$) in the hydraulic reactive polymorph of β - C_2S . Stable modification of α - C_2S is not capable of hydration and contribution to hardening of concretes and mortars.

Five binary compounds are present in the phase diagram of $SrO - Al_2O_3$ system (Fig.1). Since $4SrO \cdot Al_2O_3$ and $SrO \cdot 6Al_2O_3$ melt incongruently, there are two peritectic points. Other known strontium aluminate phases melt congruently. Five eutectic points are present in the phase diagram. Both, the eutectic and the peritectic points are invariant points without any degree of freedom (Gibbs Phase Rule, Chapter 2.1), but the system may contain thermodynamically stable melt at the temperature lower than the temperature of peritectic point. There is no stable melt present at the temperature lower than the temperature of eutectic point in the binary system.

Melt or liquid phase can be formed via congruent or incongruent melting process. Incongruent melting means the formation of peritectic melt and other solid phase. Example for strontium hexaaluminate it can be written as:



It means that the peritectic point is shifted to the left from the stoichiometric composition of strontium hexaaluminate. The peritectic liquid then contains 1 % less alumina than strontium hexaaluminate. The entire surplus of alumina stays in solid phase, therefore the temperature cannot rise if $SrO \cdot 6Al_2O_3$ solid is present (invariant point). Once $SrO \cdot 6Al_2O_3$ melts the system gets one degree of freedom and the composition of melt can change according to the line of liquidus until the rest of alumina is dissolved. The temperature as well as final composition of

melt phase can be determined by the extrapolation of $\text{SrO} \cdot 6\text{Al}_2\text{O}_3$ composition to the line of liquidus of Al_2O_3 (1920 °C, $x_{\text{SrO}}=14$ %). The liquidus line can be defined as the borderline separating heterogeneous system, which consists of precipitate and melt from the field of stability of homogeneous melt.

The ratio of formed phases can be derived by the “**lever rule**” as is described below (Al_2O_3 : peritectic melt=1 : 14). On the contrary, congruently melting strontium dialuminate forms the liquid phase of the same composition as original solid:



The melting process turns the complex structures into the melt, negative charge of $[\text{AlO}_4]^{5-}$ anions is compensated by cations of Sr^{2+} . Basic oxides also provide O^{2-} anion, that is needed for the modification of melted compounds into the simpler structures [48,49] and affects the equilibria of redox reactions (e.g. $\text{Fe}^{3+}/\text{Fe}^{2+}$ equilibrium) [50,51,52].

The system composition can be expressed by the molar or weight ratio of constituents. The rule must be fulfilled that the sum of molar (x_j) as well as weight (w_j) ratio is equal to one (or 100 %) (Eq.17), therefore $x_2=1-x_1$ or $w_2=1-w_1$ in the binary system.

$$\sum_{i=1}^j x_j = 1 \quad (17)$$

$$\sum_{i=1}^j w_j = 1 \quad (18)$$

These ratios can be recalculated one to another as follow:

$$w_i = \frac{M_i x_i}{\sum_i M_i x_i} \quad (19)$$

$$x_i = \frac{\frac{w_i}{M_i}}{\sum_i \frac{w_i}{M_i}} \quad (20)$$

where M is the molecular mass of i -th species.

The behaviour of the system during cooling of melt phase will be explained on the examples in Fig.4 with the composition given by line (1) and (2). Starting with composition (1) when

melted phase contains 90 % SrO, the first SrO solid appears at the temperature corresponding to the point A (2200 °C). The infinitesimal amount of SrO(s) (A') is in the equilibrium with the melt of composition (A). This equilibrium is described by Eq.39⁵. Using general formula of Gibbs phase law, the system has one degree of freedom. Therefore, the composition of the system may change with decreasing temperature according to the line of liquidus. Strontium oxide precipitating from the melt leads to the liquid phase enriched with Al_2O_3 (dark red arrows).

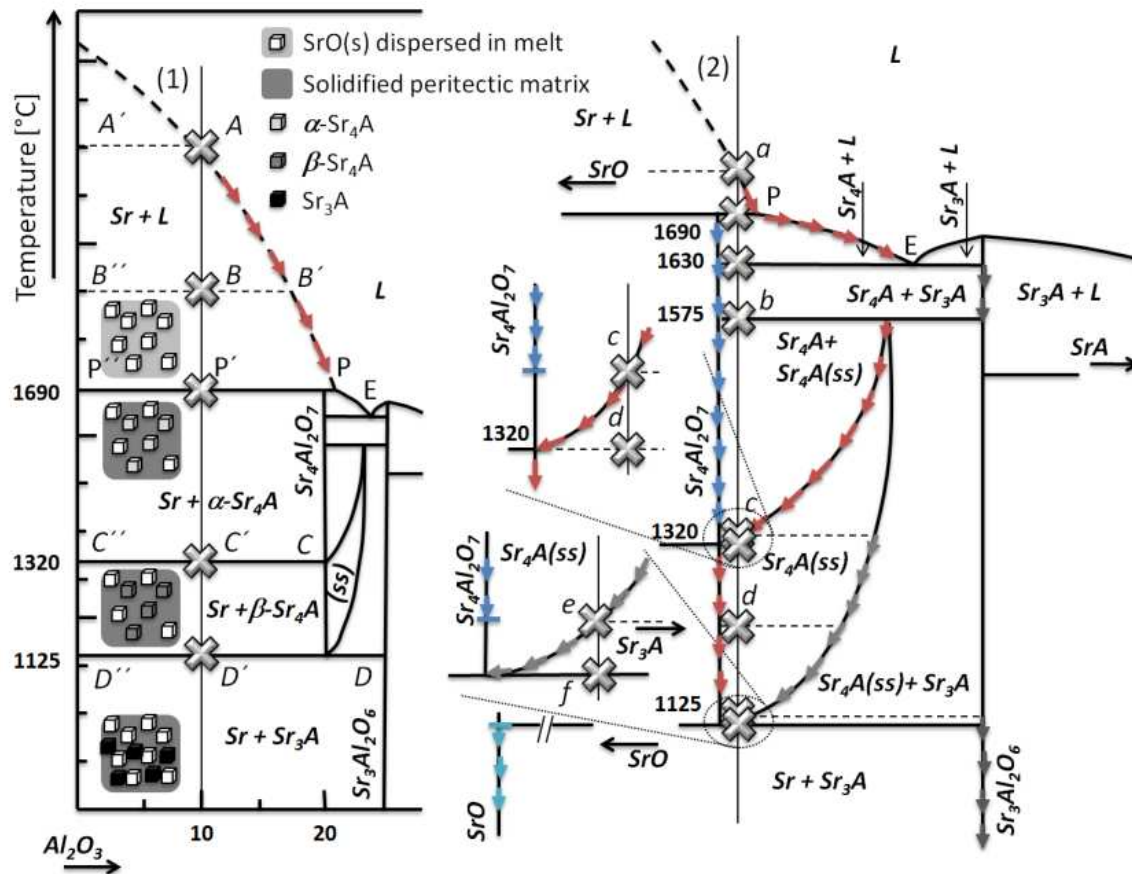


Figure 4. Crystallization pathway for the system A and B (a) with graphical illustration of "lever rule" and cooling curve.

At the temperature of 1900 °C that corresponds to the point B , the system consists of SrO(s) and melt in the ratio given by the lever rule:

$$\frac{\text{SrO(s)}}{\text{melt}} = \frac{|BB'|}{|B''B'|} \Rightarrow \text{SrO(s)} : \text{melt} = 1 : 1.3 \quad (21)$$

⁵ the line of liquidus in the phase diagram given in Fig.4 is a function of this equation, but increasing non-ideal behaviour of melt leads to the differences between experimental and calculated data as the content of the second constituent increases.

Therefore pure SrO is formed (B''), the system consists of SrO precipitate dispersed in the equilibrium melt, the composition of which is given by the line of liquidus. Three phases are present if the system reaches the composition and the temperature corresponding to the peritectic point: peritectic melt (P), tetra-strontium aluminate (Sr_4A) and strontium oxide (Sr). There is zero degree of freedom and the temperature cannot be changed until the solidification of whole melt proceeds.

Within the temperature interval from 1690 to 1320 °C, the solid system consists of strontium oxide and tetra-strontium aluminate in the ratio $|CC| : |C''C'| = 1:1$. The ratio stays unchanged to the temperature 1125°C. Below the temperature of 1125 °C, Sr_4A is decomposed to SrA and Sr_3A in the ratio 1 : 1.5.

The crystallization of the system with the composition given by line (2) begins at the temperature of point (a) where the first infinitesimal amount of strontium oxide appears. The composition of melt changes according to the line of liquidus as the temperature decreases. On the contrary in the system (1) the free strontium oxide disappears at the temperature of peritectic point (P). The Sr_4A solid and melted phase, the composition of which changes according to the line of liquidus, is the equilibrium as the temperature decreases from P to E. At the temperature of eutectic point, the system becomes invariant again and the temperature stays constant until whole eutectic melt is solidified. Sr_4A crystals appear in the fine crystallized matrix of eutectic melt, but both phases are pure crystalline phases.

Below the temperature of 1575 °C (b) the Sr_3A is dissolved in S_4A phase. Because there are three equilibrium phases (Sr_4A , $Sr_4A(ss)$ and Sr_3A) in the two component system at constant pressure, the system becomes invariant until entire Sr_3A is dissolved. Formed solid solution is being enriched by dissolved Sr_4A as the temperature decreases from point (b) to (c). That can be easily proved by the lever rule. At the temperature of point (c) Sr_4A dissolves in the solid solution and line (2) heads to the homogeneous field of solid solution, but at the temperature of 1320 °C (d) the Sr_4A phase is formed again.

Tri-strontium aluminate starts precipitating from the solid solution at the temperature of point (e) and this process continues to the temperature of point (f) where the solid solution does not exist any longer. Below this temperature, the decomposition of Sr_4A to free SrO and Sr_3A takes place.

Tri-strontium aluminate and strontium aluminate are neighboring congruently melting compounds. Therefore, they form relatively simple binary subsystem of the SrO – Al_2O_3 system that can be made as separate phase diagram (Fig.5). From this point of view, the phase diagram in Fig.1 consists of four simple systems, which are formed between oxide species and congruently melting phase or two congruently melting phases: SrO – Sr_3A , Sr_3A – SrA, SrA – SrA_2 and SrA_2 – SrA_6 .

Fig.5 shows the lever rule applied to the system containing slightly higher amount of SrO with regard to strontium aluminate stoichiometry heated to the temperature of 1600 °C. The solid to melt ratio has the value:

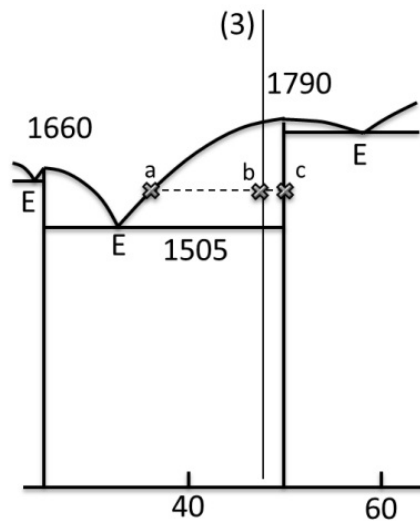


Figure 5. Binary system formed between tri-strontium aluminate and strontium aluminate.

$$\frac{\text{solid}}{\text{melt}} = \frac{|ab|}{|bc|} = \frac{47.5 - 35}{50 - 47.5} = \frac{5}{1} \quad (22)$$

The original system containing 45.7 % Al_2O_3 and $100 - 45.7 = 54.3$ % SrO consists of 1 piece of melt and 5 pieces of solid. That can be verified as follows:

Melt	Al_2O_3 [%]	35	2.5 →	1	(23)
			45.7		
Solid	Al_2O_3 [%]	50	12.5 →	5	

The same rule can be used to calculate the ratio for two systems mixed in order to reach required composition. In the case, that $x_{\text{Al}_2\text{O}_3}$ is recalculated to $w_{\text{Al}_2\text{O}_3}$ (Eq.19), the following relation can also be used for these purposes:

$$m_1 w_1 + m_2 w_2 + \dots m_i w_i = W(m_1 + m_2 + \dots m_i) \quad (24)$$

For example, if the system containing 50 % Al_2O_3 should be prepared by mixing 100 g of system with 30 % Al_2O_3 with pure Al_2O_3 (100 %), the solution is:

$$\begin{aligned} 100 \cdot 30 + m_{\text{Al}_2\text{O}_3} \cdot 100 &= 50(100 + m_{\text{Al}_2\text{O}_3}) \\ m_{\text{Al}_2\text{O}_3} &= 40 \text{ g} \end{aligned} \quad (25)$$

2.3. Calculation of melting enthalpy from equilibrium phase diagram

The equilibrium phase diagram constructed from the experimental data on the behaviour of system during heating can be used for the calculation of melting enthalpy (Δh_m) of the constituents. The solution is named as "Schröder and Le Chatelier's law" and it will be demonstrated on the SrO – Al₂O₃ diagram (Fig.1). It must be pointed out, that the following solution is derived for the equilibrium of pure crystalline solids with melt where no solid-solution is formed. That means that presented solution is applicable for all congruently melting solids in the binary system of SrO – Al₂O₃.

The liquidus line in the phase diagram represents the equilibrium state between solids and melt phase at given temperature. In the equilibrium state the chemical potential of both phases must fulfill the term:

$$\mu_{A,s}^* = \mu_{A,\ell} \quad (26)$$

where $\mu_{A,s}^*$ and $\mu_{A,\ell}$ denote the chemical potential of species A as the pure (*) solid phase (s) and in the melt (ℓ), respectively. The chemical potential of pure solids is given as follows:

$$\mu_{A,s}^* = f(T, p) \quad (27)$$

$$d\mu_{A,s}^* = \left(\frac{\partial \mu_{A,s}^*}{\partial T}\right)_p dT + \left(\frac{\partial \mu_{A,s}^*}{\partial p}\right)_T dp \quad (28)$$

$$d\mu_{A,s}^* = -s_A^* dT + v_A^* dp \quad (29)$$

where s^* and v^* are the molar entropy and volume.

The chemical potential of species A in the melt with ideal behaviour can be expressed by the equation:

$$\mu_{A,\ell} = f(T, p, x_A) \quad (30)$$

$$d\mu_{A,\ell} = -\bar{s}_{A,\ell} dT + \bar{v}_{A,\ell} dp + RT d\ln x_A \quad (31)$$

where \bar{s} and \bar{v} are partial molar entropy and volume.

With respect to Eq.26 the equilibrium state requires:

$$d\mu_{A,s}^* = d\mu_{A,\ell} \quad (32)$$

$$-s_A^* dT + v_A^* dp = -\bar{s}_{A,\ell} dT + \bar{v}_{A,\ell} dp + RT d\ln x_A \quad (33)$$

$$\left(\bar{s}_{A_l} dT - s_A^*\right) dT = \left(\bar{v}_{A_l} + v_A^*\right) dp + RT d \ln x_A \quad (34)$$

The term in the brackets corresponds to the change of entropy and volume during melting. Therefore, the applied equilibrium phase diagram is constructed for the isobaric conditions [p] which can be written:

$$\Delta s_{A,m} dT = RT d \ln x_A \quad (35)$$

where Δs_m is the melting entropy of the process, which can be expressed using the definition law of Gibbs energy for the equilibrium state (Eq.36).

$$\Delta g_m = \Delta h_m - T \Delta s_m = 0 \Rightarrow \Delta h_m = T \Delta s_m \Rightarrow \Delta s_m = \frac{\Delta h_m}{T} \quad (36)$$

From the combination of Eqs.35 and 36 the following can be derived:

$$\frac{d \ln x_A}{dT} = \frac{\Delta h_{A,m}}{RT^2} \quad (37)$$

$$\int_1^{x_A} d \ln x_A = \frac{\Delta h_{A,m}}{R} \int_{T_A}^{T_{x_A}} \frac{dT}{T^2} \quad (38)$$

$$\ln x_A = -\frac{\Delta h_{A,m}}{R} \left(\frac{1}{T_{x_A}} - \frac{1}{T_A} \right) \approx -\frac{\Delta h_{A,m}}{R} \frac{T_A - T_{x_A}}{T_A^2} \quad [x_A \rightarrow 1 \Rightarrow T_A \approx T_{x_A}] \quad (39)$$

where T_A and T_{x_A} are the melting temperature of pure species A and of the system of composition x_A , respectively. The melting (fusion) enthalpy can be assessed then from the slope (term- $\Delta h_m/R$) of plot $\ln x_A$ to be the difference ($T_{x_A}^{-1} - T_A^{-1}$).

The value T_{x_A} should be the closest possible value to T_A (x_A is close to one) due to the presumption of ideal behaviour of melted phase. In the case that the value of melting enthalpy is known, the liquidus line can be calculated from Eq.39. The example of the estimation of melting enthalpy of SrO from the equilibrium phase diagram is shown in Fig.6.

2.4. Ternary system SrO-CaO-Al₂O₃

The phase relationships of the SrO – CaO – Al₂O₃ system (Fig.7) were described by Massazza at al. [53,54]. The ternary diagram shows the formation of solid solution between corresponding EA_xA_y phases, where EA denotes alkali earth element (Ca or Sr): CaAl₁₂O₁₉ (CA₆)-

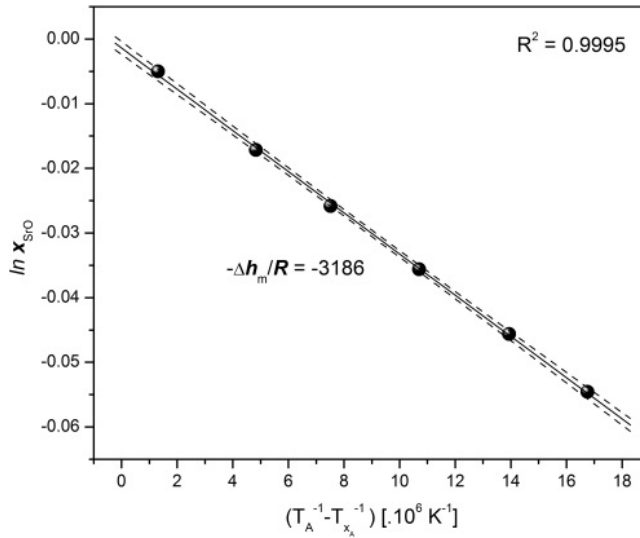


Figure 6. Estimation of melting enthalpy from phase diagram.

$\text{SrAl}_{12}\text{O}_{19}$ (SrA_6), CaAl_4O_7 (CA_2)- SrAl_4O_7 (SrA_2), CaAl_2O_4 (CA) – SrAl_2O_4 (SrA) and $\text{Ca}_3\text{Al}_2\text{O}_6$ (C_3A)- $\text{Sr}_3\text{Al}_2\text{O}_6$ (Sr_3A) [55].

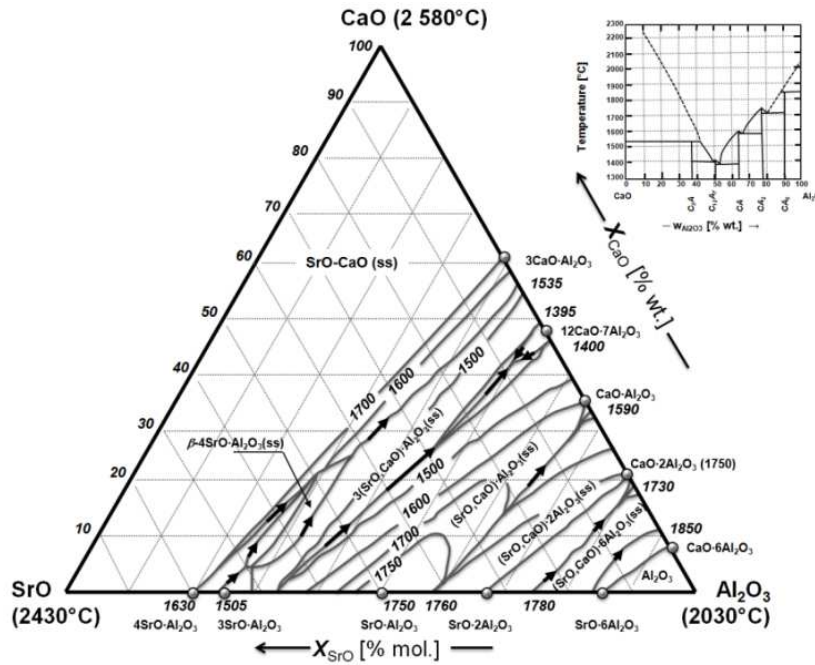


Figure 7. Phase relationship in the ternary system of CaO – SrO – Al_2O_3 [53].

The interesting fact is the stability of $\beta\text{-Sr}_4\text{A}$ solid solution up to the melting temperature in the ternary system, while in the binary system $\text{SrO} - \text{Al}_2\text{O}_3$ the $\beta\text{-Sr}_4\text{A}$ is stable only up to the temperature of 1575 °C (Fig.1).

2.5. Quaternary system CaO – SrO – Al₂O₃ – ZrO₂

The compounds formed in the system CaO – SrO – Al₂O₃ – ZrO₂ (Fig.8) are of great interest for the production of refractories due to high melting temperatures. This system contains 14 binary and ternary compounds, but the SrO – ZrO₂ system is very complicated and the literature contains contradictory information on it. The connection lines in Fig.8 divide the quaternary system into the 21 elementary tetrahedra. There are two series of continuous solid solutions CaAl₂O₄ – SrAl₂O₄ and CaZrO₃ – ZrSrO₃ [55].

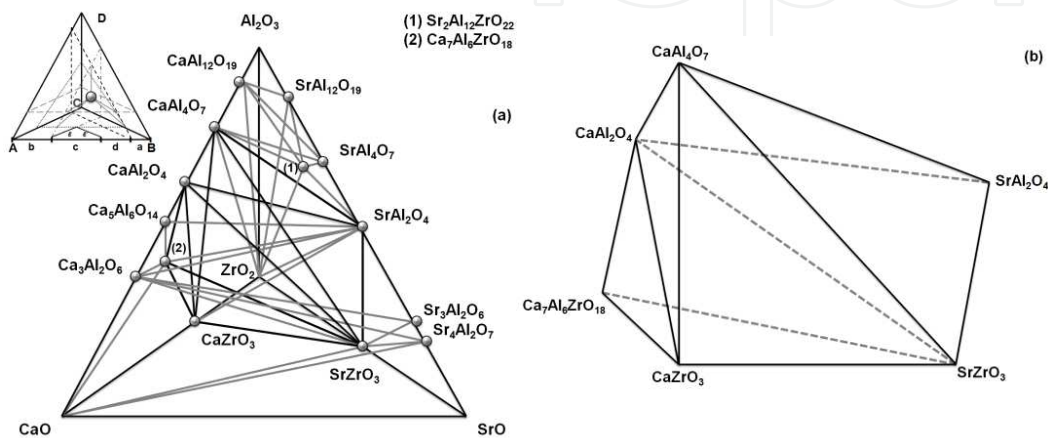


Figure 8. Elementary tetrahedra of the quaternary system CaO-SrO-Al₂O₃-ZrO₂ (a) [55] with highlighted elementary tetrahedron including CA-SrA-SrZ region (b) favourable for the production of refractory binders [56].

The region CA – SrA – SrZ is considered as favourable for the production of special cements for refractory purposes. While strontium and calcium aluminates possess the bonding properties, the calcium and strontium zirconates have high melting temperatures. These cements are characteristic of water to cement ratio from 0.20 to 0.31 and rapid hardening [56].

3. Thermodynamics of SrO-Al₂O₃ system

3.1. Estimation of molar thermal capacity

The thermal capacity of solid inorganic compounds, which are formed from elements or simple solid compounds (Eq.40), can be estimated by the Neumann-Koop rule according to the relation 41. The method is applicable for intermetallic compounds and mixed oxides.



$$c_{pm}^o(A_m B_n) = m c_{pm}^o(A) + n c_{pm}^o(B) \quad (41)$$

For example, the thermodynamic data of binary compounds from SrO – Al₂O₃ system (Fig.1) can be calculated as follows:

$$c_{pm}^{\circ}(\text{Sr}_3\text{Al}_2\text{O}_6, 298 \text{ K}) = 3 c_{pm}^{\circ}(\text{SrO}, 298 \text{ K}) + c_{pm}^{\circ}(\text{Al}_2\text{O}_3, 298 \text{ K})$$

$$c_{pm}^{\circ}(\text{SrAl}_4\text{O}_7, 298 \text{ K}) = 3 \cdot 45.241 + 79.029 = 214.752 \text{ J} \cdot \text{mol}^{-1} \text{K}^{-1} \quad (42)$$

The overview of results of other binary compounds and the comparison with experimental value is shown in Table 2. More methods can be found in literature. Kellogg [57] originally suggested a method for the estimation of heat capacity of predominantly ionic, solid compounds at 298 K. It is analogous to the Latimer's method for the estimation of standard entropies [58,59]. The method is based on the summation of contributions from the cationic and anionic groups in the compound⁶.

Binary compounds	$c_{pm}^{\circ} (25 \text{ }^{\circ}\text{C})$ [J·mol ⁻¹ ·K ⁻¹]		A	•10 ⁻³ B	•10 ⁵ C	•10 ⁻⁶ D	Difference [%]
	Estimated (a)	Determined					
4SrO•Al ₂ O ₃	259.686	253.659	308.958	36.507	-58.833	0.008	2.38
3SrO•Al ₂ O ₃	214.445	209.152	257.294	31.873	-51.243	-0.012	2.56
SrO•Al ₂ O ₃	123.963	119.030	177.192 ⁽¹⁾	4.937	-53.11	---	4.14
			146.105 ⁽²⁾	29.288	---	---	
SrO•2Al ₂ O ₃	202.685	?	269.527 ^(e)	48.85	-71.815	-9.84	---
SrO•6Al ₂ O ₃	517.572	?	707.381 ^(e)	138.6	-203.60	-30	---

(1) Temperature range 298.15 – 932 K.

(2) Temperature range 932 – 2063 K.

(a) HSC software.

(e) Results based on experimental data are not available, constants A, B, C and D were determined from estimated data.

Table 2. Estimation of molar thermal capacity of binary compounds from SrO-Al₂O₃ system from their oxides.

The temperature dependence of c_{pm}° of pure oxides in the SrO – Al₂O₃ system:

⁶ For example, the cationic contribution of Sr to heat capacity at 298 K is 25.52 J·K⁻¹. The anionic contribution for Al₂O₄ and Al₂O₆ is 98.52 and 135.46 J·K⁻¹, respectively. For strontium aluminate the heat capacities can be then calculated to be 25.52 + 98.52 = 124.04 J·mol⁻¹·K⁻¹. For tri-strontium aluminate the value 3 25.52 + 135.46 = 212.02 J·mol⁻¹·K⁻¹ at 298 K. can be found. The results show good agreement with data in Table 2.

$$c_{pm}^{\circ}(SrO, T) = 46.047 + 14.163 \cdot 10^{-3} T - \frac{3.885 \cdot 10^5}{T^2} - 7.4 \cdot 10^{-6} T^2 \quad (43)$$

[298.15 – 900 K]

$$c_{pm}^{\circ}(SrO, T) = 83.372 - 36.439 \cdot 10^{-3} T - \frac{65.775 \cdot 10^5}{T^2} + 12.175 \cdot 10^{-6} T^2 \quad (44)$$

[900 – 1700 K]

$$c_{pm}^{\circ}(Al_2O_3, T) = 109.474 + 22.414 \cdot 10^{-3} T - \frac{32.949 \cdot 10^5}{T^2} - 4.155 \cdot 10^{-6} T^2 \quad (45)$$

the c_{pm}° of binary compounds at required temperature can be calculated (Fig.9).

3.2. Estimation of enthalpy and entropy

Using the Hess' Law, the concept of formation reaction is employed for the numerical determination of enthalpy changes. In general, the reaction of the formation of pure substance B from the elements (E_i) is:

$$B = \sum v_i E_i \quad (46)$$

where v_i is the stoichiometric coefficient. The standard enthalpy of formation is defined by the formula:

$$\Delta H_{f,B}^{\circ}(T) = H_{f,B}^{\circ}(T) - \sum v_i H_{E,i}^{\circ} \quad (47)$$

Standard enthalpies of elements in their reference phases at ambient standard conditions⁷ and their reference phases are set to zero ($\Delta H_{f,i}^{\circ}=0$) [303].

Various empirical methods were developed to estimate the enthalpy of formation of mixed oxides from either the elements or the constituent binary oxides [60-63]. The Aronson's method [60], which is based on the Pauling's relation between the enthalpy of formation and the differences between the electronegativities of elements forming the compound, is the most general one:

$$\Delta H_f^{\circ} = -96.5 n_O (X' - X_O)^2 \quad [kJ \cdot mol^{-1}] \quad (48)$$

⁷ Standard ambient conditions are defined in Chapter 3.3.

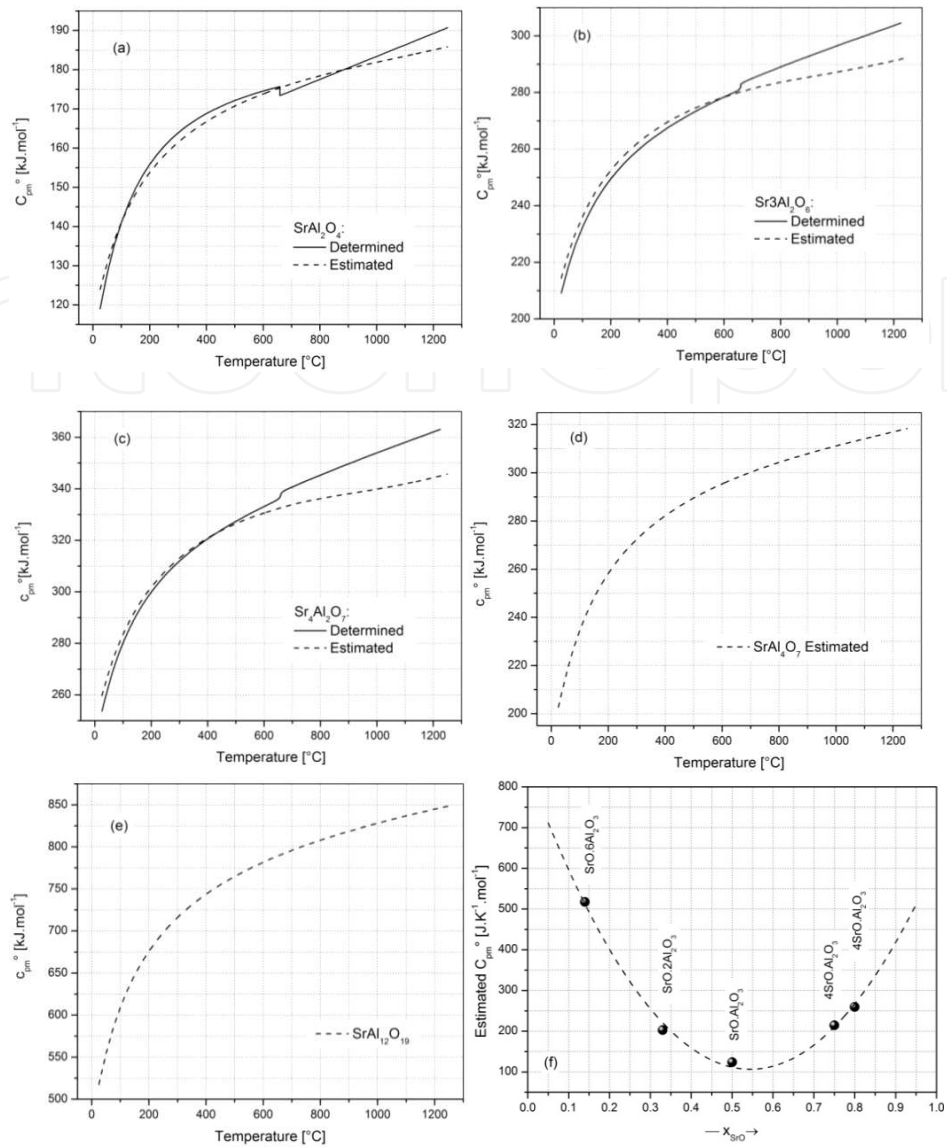


Figure 9. Temperature dependence of thermal capacity of binary compounds from SrO – Al₂O₃ system (a-e) and dependence of c_{pm}^0 on the system phase composition at temperature of 298.15 K (f).

where n_O is the number of oxygen atoms in the formula unit, X_O is the Pauling's electronegativity of oxygen and X' is the weighted geometrical mean of so-called "pseudoelectronegativities" of the oxide forming elements. The pseudoelectronegativity values are derived from known values of enthalpy of formation of relevant binary oxides. The enthalpy of formation of oxide can be then calculated as [61]:

$$X' = X_O + \sqrt{\frac{-\Delta_f H}{96.5 n_O}} \quad (49)$$

Another method, also based on the concept of electronegativity, was proposed by Zhuang et al. [62]. The method calculates the enthalpy of formation of binary oxides according to the relation:

$$\Delta_f H^0 = (n_1 + n_2) x_1 x_2 \lambda \quad (50)$$

Where n_i and x_i are the number of moles and the mole fraction of i -th constituent of mixed oxide and λ is the constant similar to the interaction parameter used in regular solution model. Assuming the formation of double oxide from the two simple oxide species:



Once the formation enthalpy is known for any double oxide $n_1(A_a O_x) n_2(B_b O_y)$, the value of λ can be calculated from the formation enthalpy of double oxide with given stoichiometry and used for oxides of another stoichiometry. Otherwise, λ can be estimated using the following formula [61,62]:

$$\lambda = -96.5 z (X_A - X_B)^2 \quad [kJ \cdot mol^{-1}] \quad (52)$$

where X_A and X_B are the Pauling's electronegativities for A and B elements and z is the stoichiometric factor (double number of oxygen atoms or ions given by oxide formula (Eq. 51)) is given by the relation:

$$z = 2 \left(\frac{x}{a} + \frac{y}{b} \right) \quad (53)$$

A new method of estimation of the enthalpy of $Al_2O_3 - Ln_2O_3$ mixed oxides formation was derived by Voňka and Leitner [61]. The method is based on the Pauling's concept of electronegativity and, in particular, on the relation between the enthalpy of formation of binary oxide and the difference between the electronegativities of the oxide-forming element and oxygen. This relation can be extended also for the calculation of enthalpy of other types of mixed oxides.

When the Pauling's electronegativity of the central cations is ≥ 1.9 , the method suggested by Šesták et al [64] enables to calculate the formation enthalpy of mixed oxide as follows:

$$\Delta_f H^0 = -29.288 M \quad (54)$$

where M is the number of oxygen atoms or ions in the double oxide. The Pauling's electronegativities of Al and Sr are 1.61 and 0.95, respectively. Therefore the assumption for Šesták method is not fulfilled in SrO – Al₂O₃ system.

Le Van [65] described the method based on the assumption of additivity of bond energies for the estimation of $\Delta_f H^\circ$:

$$\Delta_f H^\circ(298\text{ K}) = n_- P + n_+ Q + 4.184 (4n_+^2) + 4.184 n_-^2 \quad [\text{kJ} \cdot \text{mol}^{-1}] \quad (55)$$

where n_+ and n_- denote the number of cations and anions, respectively. The P and Q are characteristic parameters⁸ for cations and anions.

As was mentioned in Chapter 1.3.1, the Latimer's method of estimation of standard entropies (predominantly ionic compounds) uses the empirically found values of anion and cation contributions⁹ [58,59].

The comparison of experimental and calculated standard enthalpy of formation and the standard entropy for known binary compounds (mixed oxides) in the SrO-Al₂O₃ system is given in Table 3.

Binary compounds	$\Delta H_{f,B}^\circ(298\text{K})[\text{kJ} \cdot \text{mol}^{-1}]$		$S_m^\circ(298\text{K})[\text{kJ} \cdot \text{K}^{-1} \cdot \text{mol}^{-1}]$	
	Determined	Estimated ^(a)	Determined	Estimated ^(a)
SrO	-591.999	---	55.580	---
4SrO•Al ₂ O ₃	-4118.725	-4407.794	322.570	283.947
3SrO•Al ₂ O ₃	-3544.681	-3717.308	255.375	229.160
SrO•Al ₂ O ₃	-2338.897	-2336.337	108.800	120.219
SrO•2Al ₂ O ₃	?	-3994.452	?	180.945
SrO•6Al ₂ O ₃	?	-5424.412	?	423.852
Al ₂ O ₃	-1675.690	---	50.949	---

^(a) HSC software

Table 3. Standard enthalpy of formation and standard entropy for binary compounds in the SrO-Al₂O₃ system.

Fig.10 (a) shows that estimated value of $\Delta_f H^\circ(298\text{ K})$ is quite different from the extrapolation of fitted experimental data.

⁸ The characteristic values of $Q(\text{Sr}^{2+}) = -862$ and $P(\text{Al}_2\text{O}_4^{2-}) = -1494$ enable to estimate the formation enthalpy of strontium aluminate to be $-862 -1494 + [4.184 \cdot 42] + 4.184 = -2285 \text{ kJ} \cdot \text{mol}^{-1}$.

⁹ The anionic and cationic contributions of Sr^{2+} and $\text{Al}_2\text{O}_4^{2-}$ ions are 48.7 and 57 $\text{J} \cdot \text{K}^{-1} \cdot \text{mol}^{-1}$, respectively. The entropy of strontium aluminate can be then estimated to $52.9 + 57 = 109.9 \text{ J} \cdot \text{K}^{-1} \cdot \text{mol}^{-1}$. Using the contribution of O^{2-} for divalent cation ($2.5 \text{ J} \cdot \text{K}^{-1} \cdot \text{mol}^{-1}$), the value of $(3 \cdot 52.9) + (2 \cdot 2.5) + 57 = 220.7$.

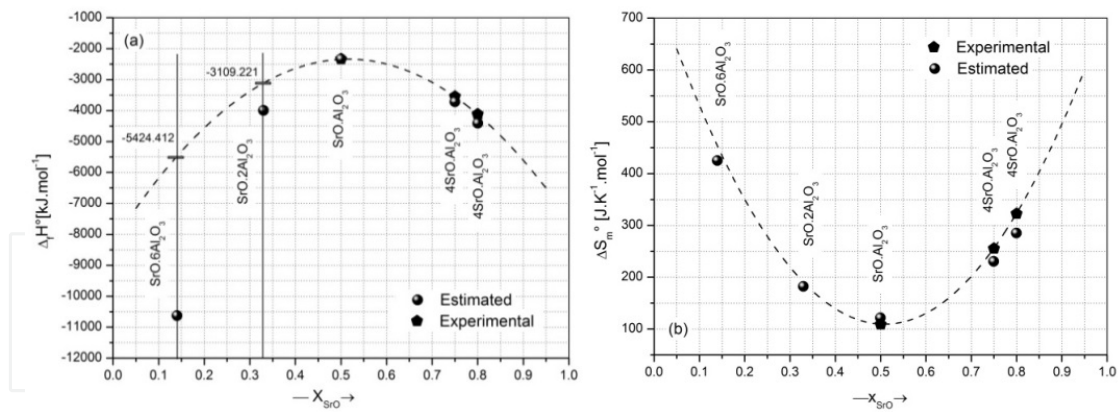


Figure 10. Estimated enthalpy (a) and entropy (b) of binary compounds in the SrO-Al₂O₃ system.

Therefore, the values expected from fitted dependence were applied for the calculation of temperature phase stability (Chapter 1.3.3). The estimated entropy (Fig.10 (b)) shows good agreement with predicted results (dashed line). The enthalpy and the entropy reach the maximum at the composition that corresponds to strontium aluminate.

The enthalpy and the entropy of species can be recalculated to required temperature using the following relations:

$$H(T) = H(298.15) + \int_{298.15}^{T_{\alpha \rightarrow \beta}} c_{pm}^{o,\alpha} dT + \Delta H_{\alpha \rightarrow \beta} + \int_{T_{\alpha \rightarrow \beta}}^T c_{pm}^{o,b} dT \quad (56)$$

$$S(T) = S(298.15) + \int_{298.15}^{T_{\alpha \rightarrow \beta}} \frac{c_{pm}^{o,\alpha}}{T} dT + \frac{\Delta H_{\alpha \rightarrow \beta}}{T} + \int_{T_{\alpha \rightarrow \beta}}^T \frac{c_{pm}^{o,b}}{T} dT \quad (57)$$

The definition law can be then used for the calculation of Gibbs energy as follows:

$$G(T) = H(T) - TS(T) \quad (58)$$

3.3. Temperature phase stability

There are five binary compounds in the phase diagram in Fig.1: 4SrO•Al₂O₃, 3SrO•Al₂O₃, SrO•Al₂O₃, SrO•2Al₂O₃ and SrO•6Al₂O₃. The thermodynamic considerations enable to evaluate the stability of these phases at given temperature. For example, all compounds mentioned above are stable at the temperature of 600 °C. This question can be solved by the

calculation of reaction Gibbs energy ($\Delta_r G^\circ$) related to the formation of compounds from simple oxides (SrO and Al_2O_3):



While the reactions 59-61 are exothermic ($\Delta_r H^\circ < 0$), the formation of $\text{SrAl}_{12}\text{O}_{19}$ is endothermic process at the temperature of 600 °C. Since $\Delta_r G^\circ < 0$ (Table 4), all these reactions lead to thermodynamically stable products. The question is, if the products are stable than basic oxides SrO and Al_2O_3 .

Eq.	$\Delta_r H^\circ$		ΔS_m	$\Delta_r G^\circ$		$\Delta_r G^{\circ(\text{bo})}$	x_{SrO}
	[kJ·mol ⁻¹]		[J·K ⁻¹ mol ⁻¹]	[kJ·mol ⁻¹]		[kJ·mol ⁻¹]	[%]
59	-75.664	EXO	47.509	-117.147	$\Delta_r G^\circ < 0$	-23.429	80.0
60	-94.403		34.681	-124.685		-31.129	75.0
61	-70.513		3.230	-73.333		-36.667	50.0
62	-54.211		17.517	-69.506		-46.337 ^(e)	33.3
63	10.342	ENDO	46.971	-30.670		-26.289 ^(e)	14.3

^(bo) The reaction Gibbs energy recalculated to one mol of basic oxides (SrO+ Al_2O_3)

^(e) Calculated from estimated thermodynamic data (Chapter 1.3.1 and 1.3.2).

Table 4. Reaction thermodynamics of the formation of binary compounds in the SrO- Al_2O_3 system at 600 °C.

The value of $\Delta_r G^\circ$ was recalculated to one mol of basic oxides $\Delta_r G^{\circ(\text{bo})}$ and plotted as the function of x_{SrO} in the compound (Fig.11(a)). The value calculated for $\text{SrO} \cdot 6\text{Al}_2\text{O}_3$ phase is placed over dashed line. That means that the compound is unstable at given conditions and should be transformed into neighboring stable phase:



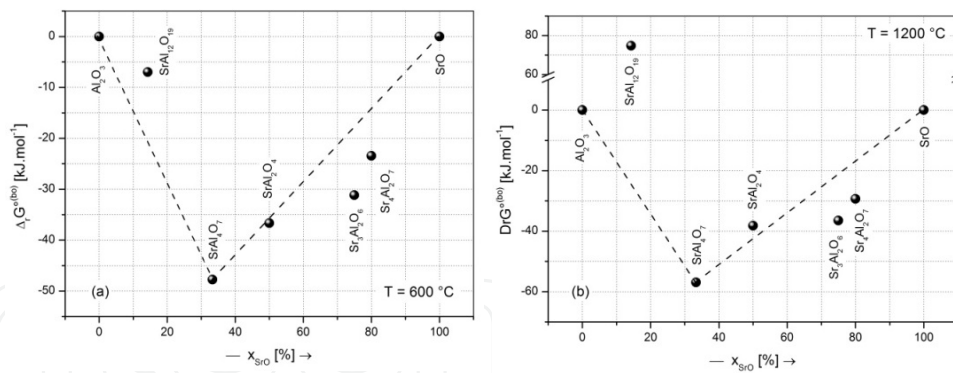


Figure 11. Thermal stability of binary compounds in the SrO – Al₂O₃ system at the temperature of 600 °C (a) and 1200 °C (b).

The negative value of $\Delta_1 G^\circ$ (-63.321 kJ) of the process provides further evidence about the thermodynamical instability of SrO·6Al₂O₃ phase¹⁰.

3.4. Equilibrium composition in ternary system

The calculation of equilibrium composition of ternary system will be demonstrated with the example for the temperature of 1000°C. The first step of this solution includes the construction of ternary plot with the points corresponding to the composition of all known phases (Fig. 12). Now it is possible to draw all possible connecting lines between all points. The intersectional points present the chemical reaction of corresponding phases.

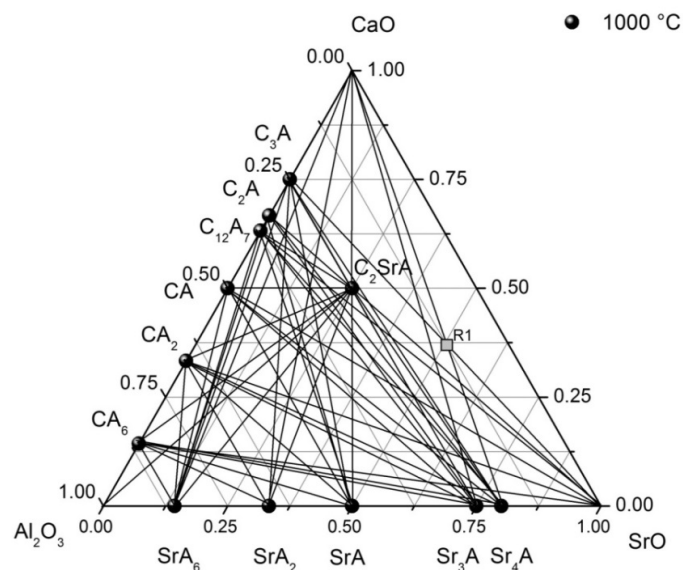


Figure 12. Possible chemical reactions in the ternary system CaO-SrO-Al₂O₃.

¹⁰ Thermal treatment of raw meal (Chapter 4) shows that formation SrA₆ is preferred from the formation of SrA₂ due to reasons discussed in Chapter 1.5.

For example, the intersectional point R1 in Fig.12, corresponds to the chemical reaction, which can be expressed by usual notation in cement chemistry as follows:



The decision, which pair of compounds is stable under given conditions (are the species on the left side of Eq.65 or the products on the right side stable?). This decision is based on the standard Gibbs energy of reactions ($\Delta_r G^\circ$) at given temperature:

$$\Delta_r H^\circ(\text{Eq.65}, 1000^\circ\text{C}) = 67\,580 \text{ J} \quad (\Delta_r H^\circ > 0 \rightarrow \text{endothermic reaction})$$

$$\Delta_r S^\circ(\text{Eq.65}, 1000^\circ\text{C}) = -7.531 \text{ J K}^{-1}$$

$$\Delta_r G^\circ(\text{Eq.65}, 1000^\circ\text{C}) = 67\,580 + (1273,13 \cdot 7.531) = 77\,168 \text{ J}$$



Therefore if $\Delta_r G^\circ > 0$, the products of reaction according to Eq.65 are thermodynamically unstable under given temperature (Eq.66) and the connection line between C_3A and Sr must be withdrawn from the diagram. These calculations should be repeated until all interconnection points are solved. The ternary diagram in Fig.13 shows the equilibrium phase composition of $\text{Al}_2\text{O}_3 - \text{SrO} - \text{CaO}$ system calculated for the temperature of 1000°C .

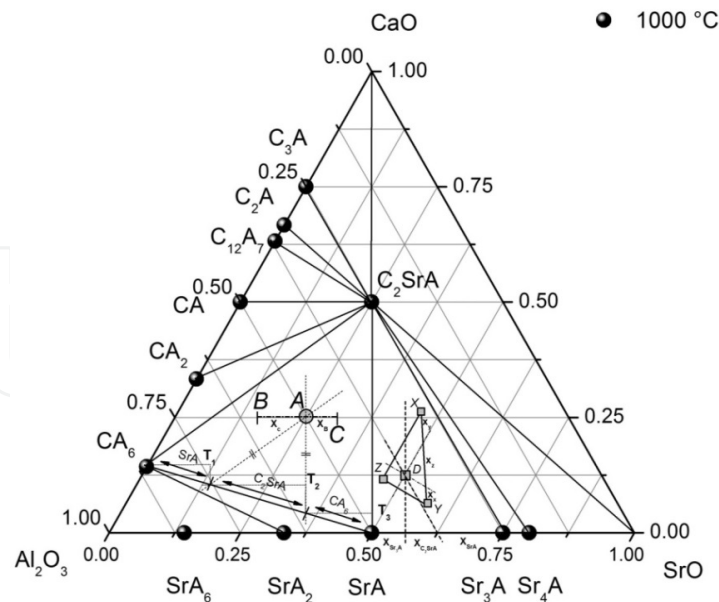


Figure 13. Phase stability in the ternary system $\text{Al}_2\text{O}_3 - \text{SrO} - \text{CaO}$ at the temperature of 1000°C .

The equilibrium ternary diagram in Fig.13 can be a useful tool to predict the phase composition of the mixture of raw materials under the thermal treatment, e.g. by thermal

treatment of mixture, the composition of which corresponds to the **point A** (50 % Al_2O_3 , 25 % SrO and 25 % CaO). This composition provides the system consisting of SrA , C_2SrA and CA_6 in the ratio 1:1.5:1. It is also possible to assess the ratio in which the constituents should be mixed in order to obtain the mixture of required composition. For example, in order to get the system A from the systems B and C, they must be mixed in the ratio $|\text{AC}| : |\text{BA}| = x_B : x_C = 1:1.55$.

Another example is the system D prepared in the corresponding ratio of systems X, Y and Z, which, after the thermal treatment to the temperature of 1000°C provides compounds SrA , Sr_3A and C_2SrA in the ratio 2.3:1:1.

4. System with chemical reaction

The number of independent chemical reactions and their stoichiometry can be derived from the Gibbs Stoichiometric Law. The system is assumed, which contains N chemical compounds consisting of M elements (C_1, C_2, \dots, C_N) where the following reaction takes place:

$$\sum_{i=1}^N \nu_i C_i = 0 \quad (67)$$

where ν_i are the stoichiometric coefficients. The reaction can be expressed in the form of matrix equation:

$$\nu^T [1, N] C [N, 1] = 0 \quad (68)$$

where ν^T is the stoichiometric coefficient matrix (1 row, N column) and C is the species matrix (N row, 1 column). The composition of chemical compounds can be expressed as:

$$\sum_{j=1}^M A_{ij} B_j = C_i \quad (69)$$

Where A_{ij} is the constitution coefficient related to the amount of atoms of j -element in the molecules of i -compounds. Therefore, it can be written:

$$A^T [N, M] B = C \quad (70)$$

Where A^T is the transposed matrix of constitution coefficient (N row, M column). The combination of Eq.70 and Eq.68 gives the following formula:

$$A^T [N, M] B = C \quad (71)$$

$$B^T Av = 0 \quad (72)$$

Since $B \neq 0$ and thus $B^T \neq 0$, the following term must be fulfilled:

$$A[M, N] v_N = 0 \quad (73)$$

For example we may consider the following system consisting of seven compounds and five elements:

$N=7$: SrCO_3 , SrO , Al_2O_3 , $\text{Al}(\text{OH})_3$, SrAl_2O_4 , CO_2 and H_2O ;

$M=5$: C, Sr, Al, O and H.

	v_1	v_2	v_3	v_4	v_5	v_6	v_7
	SrCO_3	SrO	Al_2O_3	$\text{Al}(\text{OH})_3$	SrAl_2O_4	CO_2	H_2O
C	1	0	0	0	0	1	0
Sr	1	1	0	0	1	0	0
Al	0	0	2	1	2	0	0
O	3	1	3	3	4	2	1
H	0	0	0	3	0	0	2

Table 5. Constitution coefficients in reaction system.

Via the substitution from the table of constitution coefficients (Table 5) to Eq.73, the following expression should be derived:

$$\begin{bmatrix} 1 & 0 & 0 & 0 & 0 & 1 & 0 \\ 1 & 1 & 0 & 0 & 1 & 0 & 0 \\ 0 & 0 & 2 & 1 & 2 & 0 & 0 \\ 3 & 1 & 3 & 3 & 4 & 2 & 1 \\ 0 & 0 & 0 & 3 & 0 & 0 & 2 \end{bmatrix} \begin{bmatrix} v_1 \\ v_2 \\ v_3 \\ v_4 \\ v_5 \\ v_6 \\ v_7 \end{bmatrix} = \begin{bmatrix} 0 \\ 0 \\ 0 \\ 0 \\ 0 \end{bmatrix} \quad (74)$$

The order of matrix A $[M,N]$ can be now determined¹¹:

$$\begin{bmatrix} 1 & 0 & 0 & 0 & 0 & 1 & 0 \\ 1 & 1 & 0 & 0 & 1 & 0 & 0 \\ 0 & 0 & 2 & 1 & 2 & 0 & 0 \\ 3 & 1 & 3 & 3 & 4 & 2 & 1 \\ 0 & 0 & 0 & 3 & 0 & 0 & 2 \end{bmatrix} \Rightarrow \begin{bmatrix} 1 & 0 & 0 & 0 & 0 & 1 & 0 \\ 0 & 1 & 0 & 0 & 1 & -1 & 0 \\ 0 & 0 & 1 & \frac{1}{2} & 1 & 0 & 0 \\ 0 & 0 & 0 & 1 & 0 & 0 & \frac{2}{3} \\ 0 & 0 & 0 & 0 & 0 & 0 & 0 \end{bmatrix} \quad (75)$$

The last row of matrix A is a linear combination of other rows and the order of matrix of constitution coefficients (h) is equal to 4. From the **Gibbs Stoichiometric Law** the following can be now calculated:

$$R = N - h = 7 - 4 = 3 \quad (76)$$

Therefore, there are three independent chemical reactions in the system. Eq.74 and the solution 75 lead to the following results:

$$v_1 + v_6 = 0 \quad (77)$$

$$v_1 + v_2 - v_6 = 0 \quad (78)$$

$$v_3 + \frac{1}{2}v_4 + v_5 = 0 \quad (79)$$

$$v_4 + \frac{2}{3}v_7 = 0 \quad (80)$$

The stoichiometry of these processes can be calculated choosing three parameters:

a. The choice $v_7=1$, $v_6=0$ and $v_5=0$ leads to the solution:

$$v_4 = -\frac{2}{3} \quad (81)$$

¹¹ Except for the switch of the row with column (order of column must remain unchanged), all usual mathematical operation can be used. These calculation includes: The change of the order of row (1), The multiplication of row by a constant (2), The summation of row with other row or their linear combination (3), The exclusion of row which is a linear combination of other rows (e.g. last row in Eq.75).

$$v_3 = \frac{1}{3} \quad (82)$$

$$v_2 = 0 \quad (83)$$

$$v_1 = 0 \quad (84)$$



From the calculation of the reaction Gibbs energy it can be estimated, that the reaction 85 proceeds to right side (product) if the temperature is lower than 113 °C ($\Delta_r G < 0$) and further, the dehydration of gibbsite takes place if the temperature is higher ($\Delta_r G > 0$).

b. The choice $v_7=0$, $v_6=1$ and $v_5=0$ leads to the solution:

$$v_4 = 0 \quad (86)$$

$$v_3 = 0 \quad (87)$$

$$v_2 = 1 \quad (88)$$

$$v_1 = -1 \quad (89)$$



This reaction reaches the equilibrium state at the temperature of 1071°C ($\Delta_r G=0$).

c. The choice $v_7=0$, $v_6=0$ and $v_5=1$ enables to find the last independent reaction in the system where $v_4=0$, $v_3=0$, $v_2=1$ and $v_1=-1$:



The formation of strontium aluminate from the oxide species (Eq.91), the thermal decomposition of gibbsite (Eq.85) and strontium carbonate (Eq.90) are three independent reactions in the above mentioned system. The solution represents the base vectors (v_1, v_2, v_3) of 3D reaction space ($N-h=3$) which come through the beginning of 7D (N) vector space:

Eq.85: (001);

Eq.90: (-110);

Eq.91: (0-1-1).

All other solutions are their linear combinations. All these reactions also increase the value of parameter C in Eq.1.9.

The system base consists of first ($N-h$) species in Table 5. Therefore, we can choose different order of species and solve different three independent reactions. The number of possible system bases in this system can be calculated from the equation:

$$\binom{N}{h} = \frac{N!}{h!(N-h)!} = \frac{7!}{4!3!} = 35 \quad (92)$$

For example, if we rearrange the system as follows (system base is marked bold):

SrAl_2O_4 , SrO , H_2O , CO_2 , $\text{Al}(\text{OH})_3$, SrCO_3 , Al_2O_3 ,

the following independent reaction is determined:

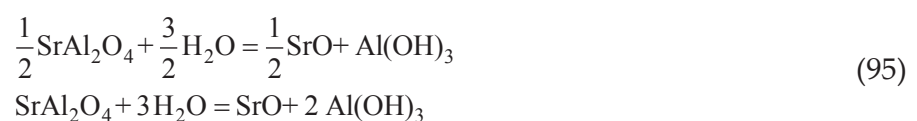
d. The choice $v_7=1$, $v_6=0$ and $v_5=0$ leads to the solution:



e. The choice $v_7=0$, $v_6=1$ and $v_5=0$ leads to the solution:



f. The choice $v_7=0$, $v_6=0$ and $v_5=1$ leads to the solution:



But not all possible system bases are valid; the stoichiometry of independent reaction can be calculated only from the system base that contains all elements occurring in the system. For example the choice:



is not acceptable, because the compounds in the system base do not contain hydrogen.

In order to better explain the geometric meaning of the Gibbs Stoichiometric Law, the following simple reaction system is applied:

- $N=3$: SrO, Al₂O₃ and SrAl₂O₄.
- $M=3$: Sr, Al and O.

$$\begin{array}{c} v_1 \quad v_2 \quad v_3 \\ \text{Sr} \quad \begin{bmatrix} 1 & 0 & 1 \end{bmatrix} \\ \text{Al} \quad \begin{bmatrix} 0 & 2 & 2 \end{bmatrix} \\ \text{O} \quad \begin{bmatrix} 1 & 3 & 4 \end{bmatrix} \end{array} \begin{bmatrix} v_1 \\ v_2 \\ v_3 \end{bmatrix} = \begin{bmatrix} 0 \\ 0 \\ 0 \end{bmatrix} \quad (96)$$

$$\begin{bmatrix} 1 & 0 & 1 \\ 0 & 2 & 2 \\ 1 & 3 & 4 \end{bmatrix} \Rightarrow K \Rightarrow \begin{bmatrix} 1 & 0 & 1 \\ 0 & 1 & 1 \\ 0 & 0 & 0 \end{bmatrix} \Rightarrow h = 2 \quad (97)$$

$$R = N - h = 3 - 2 = 1 \quad (98)$$

Therefore we search for only one independent reaction, where $v_3=1$:

$$v_2 = -v_3 = -1 \quad (99)$$

$$v_1 = -v_3 = -1 \quad (100)$$



The results represent the coordinates vector (-1-11) related to the line passing through the beginning P[0,0,0] of 3D reaction space (Fig.14). As results from Eq.92, there are three options for the system base.

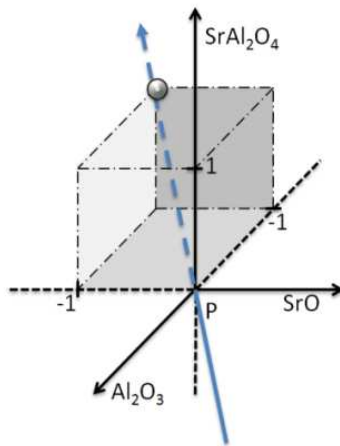


Figure 14. Geometric drawing of the solution resulting from the Gibbs Stoichiometric Law.

5. Density of cement phases

The densities of cement phases are fundamental parameter with many uses, such as calculating the space filling in pastes by solid cement substances as well as the assessment of the potential for changes of size and porosity within hardened pastes undergoing the phase changes. The substances containing cement can be divided into two groups: crystalline and amorphous. The principal amorphous substance of Portland cement is C-S-H. It poses certain problems in determining its density as it is insufficiently crystalline for the application of conventional crystallographic methods: only experimentally-determined measurements are useful. Crystalline solids, on the other hand, are amenable for the calculation of density from crystallographic constants using the relationship [66]:

$$\rho = \frac{ZM}{N_A V} \quad [\text{kg} \cdot \text{m}^{-3}] \quad (102)$$

where ρ is the calculated density, Z is the number of formula units per unit cell, M is the formula weight, V is the unit cell volume ($V=M/\rho$) and $N_A=6.02214 \cdot 10^{23} \text{ mol}^{-1}$ is the Avogadro's number.

The volumes of the unit cell can be calculated as follows:

- Isometric /cubic crystal system: $V=a^3$;
- Tetragonal crystal system: $V=a^2c$;
- Orthorhombic crystal system: $V=abc$;
- Hexagonal /trigonal crystal system: $V=a^2c \sin (60^\circ)$;

- Monoclinic crystal system: $V=abc \sin (\beta)$;
- Triclinic crystal system: $V=abc \sin ((1-\cos^2\alpha - \cos^2\beta - \cos^2\gamma)+2(\cos \alpha \cos \beta \cos \gamma))^{1/2}$

where a, b, c are the unit cell axial dimensions and α, β, γ are the relevant angles. The parameters of basic seven lattice systems are shown in Fig.15.

Phase in SrO-Al ₂ O ₃ system	Sr ₃ A 3SrO·Al ₂ O ₃		SrA SrO·Al ₂ O ₃		α-SrA ₂ SrO·2Al ₂ O ₃	
Crystal system	Cubic		Monoclinic		Monoclinic	
M [kg·mol ⁻¹]	0.41282		0.20558		0.30754	
Z	24		4		4	
a [m]	1.586·10 ⁻⁹		5.150·10 ⁻¹⁰		1.304·10 ⁻⁹	
b [m]	---		8.836·10 ⁻¹⁰		9.011·10 ⁻¹⁰	
c [m]	---		8.442·10 ⁻¹⁰		5.536·10 ⁻¹⁰	
β [°]	---		93.43		106.12	
V [m ³]	3.986·10 ⁻²⁷		3.384·10 ⁻²⁸		6.249·10 ⁻²⁸	
ρ [kg·m ⁻³]	4127		3561		3269	
Phase in SrO-Al ₂ O ₃ system	β-SrA ₂ SrO·2Al ₂ O ₃		SrA ₆ SrO·6Al ₂ O ₃		Sr ₁₀ A ₃ 10SrO·3Al ₂ O ₃	
Crystal system	Orthorhombic		Hexagonal		Monoclinic	
M [kg·mol ⁻¹]	0.30754		0.71539		1.34208	
Z	4		2		8	
a [m]	8.085·10 ⁻¹⁰		5.562·10 ⁻¹⁰		3.558·10 ⁻⁹	
b [m]	1.185·10 ⁻⁹		---		7.846·10 ⁻¹⁰	
c [m]	4.407·10 ⁻¹⁰		2.197·10 ⁻⁹		1.575·10 ⁻⁹	
β [°]	---		60		103.68	
V [m ³]	4.220·10 ⁻²⁸		5.886·10 ⁻²⁸		4.272·10 ⁻²⁷	
ρ [kg·m ⁻³]	4840		4036		4174	

Table 6. Calculation of the density of strontium aluminate cement phases.

Some examples including calculated volume and the density of compounds from SrO – Al₂O₃ system are given in Table 6.

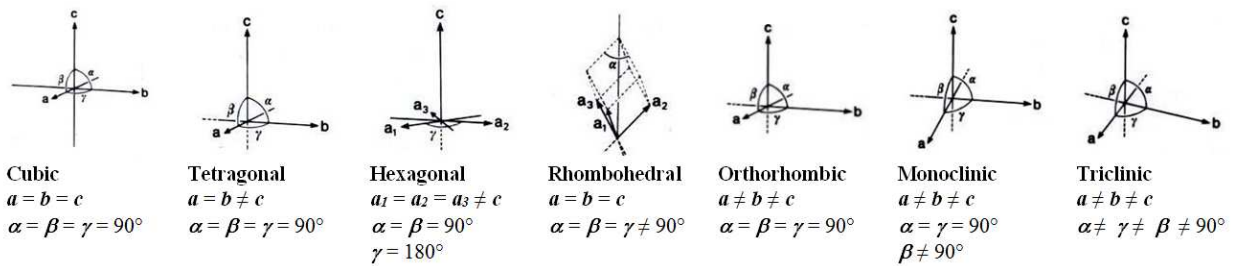


Figure 15. Parameters of basic lattice system.

Calculated data from Table 6 enable to explain how the density of compounds formed in the binary system of SrO-Al₂O₃ depends on the SrO/ Al₂O₃ ratio. Fig.16(a) shows that there are two exponential functions, which are cross each other in the composition corresponding to the SrA₂ phase (please consult with Fig.11).

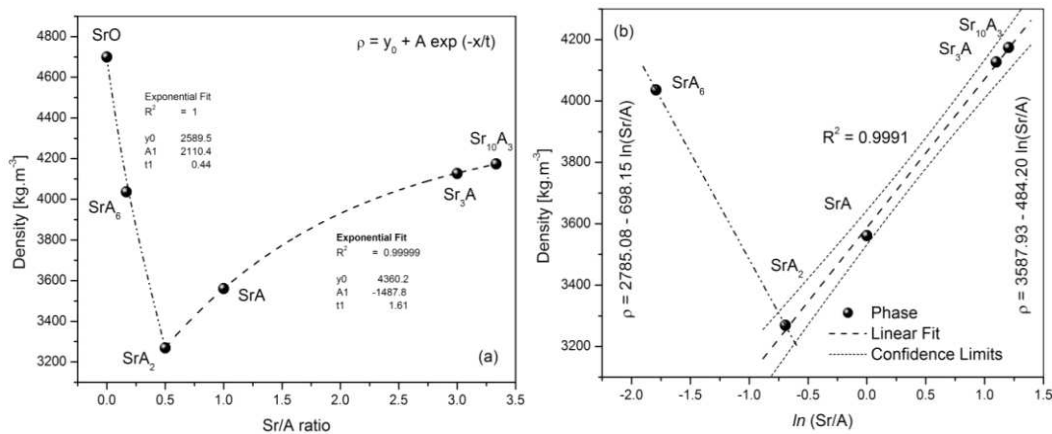


Figure 16. The influence of Sr/A ratio on the density (a) and its linearized dependence (b).

These exponential functions should be linearized as is shown in Fig.16(b). It is also a possible reason, why the formation of SrA₆ phase is preferred from the formation of SrA₂; lesser energy is required for the deformation of surroundings by newly formed crystal. Therefore the phase should be prepared via precipitation from melt, but the solid state synthesis is difficult [67,68].

6. Kinetics of heterogeneous processes

Since the thermal decomposition of solids is the most significant field of heterogeneous kinetics, the common analytical techniques include the methods such TG, DTA, DSC, TDA, etc., but other techniques could be also used by kinetic methods. These measurements are usually applied for the investigation of kinetics and mechanism of heterogeneous processes using the data measured as the function of time or temperature [69,70].

6.1. Mechanism dependent methods

Mechanism dependent or reaction model fitting method should be divided into two large groups [63,67]:

- Isothermal method;
- Non-isothermal method.

Both use the reaction models, which describe the dependence of degree of conversion (fractional conversion or the extent of conversion, α) on time (isothermal method) or temperature (non-isothermal method). The reaction model usually refers to the rate limiting step of process and the reaction system geometry (Table 7)

The fractional conversion is usually defined as the ratio of some system additional properties (mass, length, area...), the change of volume or mass of the system are mostly used:

$$\alpha = \frac{N_0 - N_t}{N_0 - N_\infty} \quad (103)$$

where N_0 , N_t and N_∞ are the initial value, the value reached in time t and the final value, respectively. The value α is normalized in the range from 0 to 1 (or 0 to 100 %).

The following differential kinetic equation was used for the description of kinetics of investigated process via the **isothermal method** [71-73,456].

$$\frac{d\alpha}{dt} = k(T) \cdot f(\alpha) \quad (104)$$

The integration of Eq.104 leads to the formula:

$$\int_0^\alpha \frac{d\alpha}{f(\alpha)} = k \cdot \int_{t=0}^t dt \Rightarrow g(\alpha) = kt \quad (105)$$

where k is the constant of reaction rate. In the case that correct kinetic function was applied, the plot of $g(\alpha)$ versus t provides straight line. The rate constant k can be then calculated as the slope of this plot.

The value of k for several temperatures must be determined for the calculation of activation energy (E_a) and frequency factor (A) via the logarithmic form (Eq.107) of Arrhenius law (Eq. 106):

$$k = A \exp\left(-\frac{E_a}{RT}\right) \quad (106)$$

$$\ln k = \ln A - \frac{E_a}{R} \frac{1}{T} \quad (107)$$

where R denotes the universal gas constant ($8.314 \text{ J} \cdot \text{K}^{-1} \cdot \text{mol}^{-1}$) and other symbols have their usual meaning. The plot (so-called Arrhenius plot) of $\ln k$ versus T^{-1} provides straight line with the slope $-E_a/R$ and the intercept with y -axis equal to $\ln A$. Several experiments should be performed in order to obtain the line with insufficient number of points, which enables to determine reliable slope of the Arrhenius plot (please see Fig.18 in Chapter 4 for example of Arrhenius plot).

Sign.	$f(\alpha)$	$g(\alpha) = kt$	Name of kinetic function	Rate limiting step	Description	
$F_{1/3}$	$(3/2)(1-\alpha)^{1/3}$	$1-(1-\alpha)^{2/3}$	One-third order		Chemical process or mechanism non-invoking equations	
$F_{3/4}$	$4(1-\alpha)^{3/4}$	$1-(1-\alpha)^{1/4}$	Three-quarters order			
$F_{3/2}$	$2(1-\alpha)^{3/2}$	$(1-\alpha)^{-1/2} - 1$	One and half order	Chemical reaction		
F_2	$(1-\alpha)^2$	$(1-\alpha)^{-1} - 1$	Second order			
F_3	$(1/2)(1-\alpha)^3$	$(1-\alpha)^{-2} - 1$	Third order			
$P_{3/2}$	$(2/3)\alpha^{-1/2}$	$\alpha^{3/2}$	Mampel power law	Nucleation	Acceleratory rate equations	
$P_{1/2}$	$2\alpha^{1/2}$	$\alpha^{1/2}$				
$P_{1/3}$	$3\alpha^{2/3}$	$\alpha^{1/3}$				
$P_{1/4}$	$4\alpha^{3/4}$	$\alpha^{1/4}$				
E_1	α	$\ln \alpha$	Exponential law			
A_1, F_1	$1-\alpha$	$-\ln(1-\alpha)$	KJMA or JMAYK (Johanson-Mehl-Avrami-Yerofeyev-Kolgomorov equation)	Random nucleation	$n=1$	
$A_{3/2}$	$3/2(1-\alpha)[-\ln(1-\alpha)]^{1/3}$	$[-\ln(1-\alpha)]^{2/3}$			$n=3/2$	Sigmoidal rate equations or
A_2	$2(1-\alpha)[-\ln(1-\alpha)]^{1/2}$	$[-\ln(1-\alpha)]^{1/2}$			$n=2$	random
A_3	$3(1-\alpha)[-\ln(1-\alpha)]^{2/3}$	$[-\ln(1-\alpha)]^{1/3}$			$n=3$	nucleation and
A_4	$4(1-\alpha)[-\ln(1-\alpha)]^{3/4}$	$[-\ln(1-\alpha)]^{1/4}$			$n=4$	subsequent growth
A_u	$\alpha(1-\alpha)$	$\ln[\alpha/(1-\alpha)]$	Prout-Tomkins equation	Branching nuclei		
R_1	$(1-\alpha)^0$	α	Power law	Contracting disc	Phase boundary	
R_2	$2(1-\alpha)^{1/2}$	$1-(1-\alpha)^{1/2}$		Contracting cylinder	deceleratory rate equations	
R_3	$3(1-\alpha)^{2/3}$	$1-(1-\alpha)^{1/3}$		Contracting sphere		
D_1	$1/2\alpha$	α^2	Parabola law	1D diffusion	Diffusion limited	
D_2	$[-\ln(1-\alpha)]^{-1}$	$\alpha + (1-\alpha)\ln(1-\alpha)$	Valensi equation	2D diffusion	deceleratory reaction	
D_3	$3/2(1-\alpha)^{2/3}[1-(1-\alpha)^{1/3}]^{-1}$	$[1-(1-\alpha)^{1/3}]^2$	Jander equation	3D diffusion		

Sign.	$f(\alpha)$	$g(\alpha) = kt$	Name of kinetic function	Rate limiting step	Description
D_4	$3/2[(1-\alpha)^{-1/3}-1]^{-1}$		Ginstling-Brounstein equation		
D_5	$3/2(1-\alpha)^{4/3}[(1-\alpha)^{-1/3}-1]^{-1}$		Zhuravlev, Lesokin, Tempelman eq.		
D_6	$3/2(1+\alpha)^{2/3}[(1+\alpha)^{1/3}-1]^{-1}$		anti-Jander eq.		
---	$3/2 [(1+\alpha)^{1/3}-1]^{-1}$		anti- Ginstling-Brounstein eq.		
---	$3/2(1+\alpha)^{4/3}[(1+\alpha)^{-1/3}-1]^{-1}$		anti- Zhuravlev, Lesokin, Tempelman eq.		

Table 7. Overview of known kinetic functions representing applied kinetic model for the process.

The non-isothermal method enables to determine the kinetic parameters of the process from one experiment¹², therefore it is sometime termed as the single run method. The non-isothermal method is based on the assumption that the kinetics of processes should be described by the constitutive formula Eq.104. The function $f(\alpha)$ depends on applied kinetic model (Table 7) and the temperature dependence of the rate constant $k(T)$ is given by the Arrhenius law (Eq.106).

If the constant heating rate (CHR methods) Θ is applied, i.e. $dT=\Theta dt$, the combination of Eqs. 106 and 107 leads to the relationship [73-75,87]:

$$\frac{d\alpha}{f(\alpha)} = \frac{A}{\Theta} \cdot \exp\left(-\frac{E_a}{RT}\right) dT \quad (108)$$

The integration of Eq.108 yields to the formula:

$$g(\alpha) \cong \frac{AE_a}{\Theta R} \cdot p(x) \quad (109)$$

where the function $g(\alpha)$ represents the kinetic function and A , E_a , R and Θ are the temperature independent parameters. The determination and accurate calculation of the $p(x)$ function is a marginal problem in the non-isothermal kinetic [64]. The Coats and Redfern approximation of the $p(x)$ function is usually used [76].

$$\ln\left(\frac{g(\alpha)}{T^2}\right) = \left[\ln \frac{AR}{\Theta E_a} \left(1 - \frac{2RT}{E_a}\right) \right] - \frac{E_a}{R} \cdot \frac{1}{T} \cong \ln\left(\frac{AR}{\Theta E}\right) - \frac{E_a}{R} \cdot \frac{1}{T} \quad (110)$$

¹² As was demonstrated in Chapter 4.2.1.

A straight line was obtained by plotting $\ln[g(\alpha)/T^2]$ versus reciprocal temperature (T^{-1}) for correct mathematical model $g(\alpha)$ of the reaction mechanism. The overall activation energy and pre-exponential factor were calculated from the slope and the intercept with y-axis of the plot, respectively.

The expression of $p(x)$ according to Schlomilch can be written as [77,456]:

$$p(x) = \exp\left(-\frac{E_a}{RT}\right) \left(\frac{1}{x}\right) \left(\frac{1}{x+2}\right) \quad (111)$$

6.2. Model free methods

The Kissinger's kinetic approach is simple and often applied kinetic equation [78,79]:

$$\ln\left[\frac{\Theta}{T_m^2}\right] = \ln\left[\frac{AR}{E_a} n(1-\alpha_m)^{n-1}\right] - \frac{E_a}{RT_m} = \text{const.} - \frac{E_a}{RT_m} \quad (112)$$

where T_m is the peak temperature measured under applied heating rate Θ , n is the empirical reaction order (kinetic exponent), α_m is the fractional conversion reached for the temperature T_m and R is the universal gas constant. The plot of $\ln(AR/E_a)$ versus T_m^{-1} was fitted by the straight line with the slope equal to $-E_a/R$ whereas the intercept yielded to the constant term of Eq.112.

The peak methods approximate the fixed state of reaction to the stage at which the maximum rate of the process is achieved, i.e. to the peak of thermoanalytical curve. It must be pointed out that the Kissinger approach can be used for the rate (differential)-isoconversion (Friedman or FR-[80]) type as well as for the $p(y)$ -isoconversion methods in principle, but the method's popularity place the Eq.112 into a group of maximum rate methods [81].

6.3. Estimation of the mechanism of process

The mechanism was estimated from the shape of DTG peak via the value of kinetic exponent (n) which was related to the empirical order of reaction [78,82] The exponent can be calculated from the equation [83,84]:

$$n = \frac{2.5 R T_m^2}{w_{1/2} E_a} \quad (113)$$

where $w_{1/2}$ is the half-width (width at a half high) of peak. The value of kinetic exponent is typical for various mechanisms of investigated process [85].

Based on the foundation that the peak asymmetry increases with decreasing value of n Kissinger [78] has proposed the method that uses the shape index (SI) of TA curve peak that can be analytically expressed as:

$$SI = \frac{\left(\partial^2 N/\partial t^2\right)_{T_1}}{\left(\partial^2 N/\partial t^2\right)_{T_2}} \quad (114)$$

where N denotes the value of measured property, t is the time, T_1 and T_2 are the first (frontal) and second (terminal) inflection point, respectively. The shape index is only the function of reaction order.

The value of kinetic exponent can be then calculated according to the first [78] and the second Kissinger approach [76]:

$$n_{K1} = 1.26 SI^{1/2} \quad (115)$$

$$n_{K2} = 1.88 SI \quad (116)$$

6.4. Thermodynamic consideration

The correlation between kinetic and thermodynamic parameters of the investigated process results from the combination of Arrhenius with Eyring or Wertera and Zenera laws related to the temperature dependence of rate constant ($k(T)$) [86]:

$$\begin{aligned} k(T) &= A \exp\left[-\frac{E_a}{RT}\right] = \frac{k_B T}{h} \exp\left[\frac{\Delta S^\ddagger}{R}\right] \exp\left[-\frac{\Delta H^\ddagger}{RT}\right] \\ &= \nu \exp\left[-\frac{\Delta G^\ddagger}{RT}\right] = \nu K^\ddagger \end{aligned} \quad (117)$$

where k_B , h and $\nu=k_B T/h$ are the Boltzmann, the Plank constant and the vibration frequency, respectively. The thermodynamic parameters of activated complex, including free energy (ΔG^\ddagger), enthalpy (ΔH^\ddagger) and entropy (ΔS^\ddagger) of the process were calculated using Eyring equations [86,87,88]:

$$\Delta H^\ddagger = E_{a,\alpha} - RT_\alpha \quad (118)$$

$$\Delta S^\ddagger = R \left[\ln \left(\frac{h A_\alpha}{k_B T_\alpha} \right) - 1 \right] \quad (119)$$

$$\Delta G^\# = \Delta H^\# - T_\alpha \Delta S^\# \quad (120)$$

The thermodynamic parameters of activated complex are often calculated using the peak temperature T_m so that the value of $\Delta G^\#$, $\Delta H^\#$ and $S^\#$ is related to the highest rate of process.

6.5. Calculation of theoretical value of activation energy

The approach is known as the "Congruent dissociative vaporization mechanism" (CDV). In the case of a solid compound S decomposed into gaseous products A and B with simultaneous condensation of low-volatility of species A , that is [89,369]:



The theoretical value of activation energy E_a^T should be different for equimolar (in the absence of gaseous product B in the reactor atmosphere) and isobaric (in the presence of the excess of gaseous product B) modes of decomposition. The relations for the equimolar (E_a^{Te}) mode are:

$$E_a^{Te} = \frac{\Delta_{rc} H^\circ(T)}{\nu} = \frac{\Delta_r H^\circ(T)}{a+b} \quad (122)$$

and for the isobaric mode (E_a^{Ti}) they are:

$$E_a^{Ti} = \frac{\Delta_{rc} H^\circ(T)}{\nu-b} = \frac{\Delta_r H^\circ(T)}{a} \quad (123)$$

$$\Delta_r H^\circ(T) = \sum \nu_i \Delta_f H_i^\circ \quad (124)$$

ν denotes total number of moles of gaseous product ($a+b$) and $\Delta_r H^\circ$ is the reaction enthalpy for given temperature (Eq.124). The temperature dependence of enthalpy is given by Eq.21 in Chapter 4. In both cases, the E_a^T parameter corresponds to the specific enthalpy, i.e. the enthalpy of the decomposition reaction reduced to one mole of primary products without including components present in excess.

In order to take into account the partial transfer of energy released in the condensation of low-volatility product A to the reactant, the calculations of enthalpy of decomposition reaction 121 require an additional term ($\tau a \Delta_c H^\circ(A,T)$) where the coefficient τ corresponds to the fraction of condensation energy transferred to the reactant at the interface. The reaction enthalpy is then given by the relation:

$$\begin{aligned} \Delta_{rc}H^{\circ}(T) &= a \Delta_fH^{\circ}(A,T) + b \Delta_fH^{\circ}(B,T) \\ &- c \Delta_fH^{\circ}(C,T) + \tau a \Delta_cH^{\circ}(A,T) \end{aligned} \quad (125)$$

For the majority of substances, the condition $\tau=0.5$ can be applied [89,90].

An essential difference between the CDV mechanism and the Arrhenius activation mechanism is that during the interface reactions, a proportion of the energy released on condensation of a non-volatile product is transferred to the solid reactant, reducing the energy barrier for further reactant volatilization. Thus, 'recycled' energy is responsible for the autocatalytic behaviour, justifying the following important generalizations [70]:

- Models identifying the preferred occurrence of chemical change at reactant/product contact interfaces with (uncharacterized, qualitative) 'strain', 'catalysis of by product', etc., can now be discarded as providing no insights into the reaction controls and mechanisms.
- Autocatalytic behaviour, resulting from the redistribution of product condensation energy, occurs when the decomposition proceeds at a reactant/product contact interface. Reactions yielding non-condensed (non-volatile) product transfer no energy, so that $\tau=0$.
- Because the energy transfer is responsible for the autocatalysis, the variations in τ , found for a number of diverse substances, are identified with supersaturation of the non-volatile component rather than the chemical properties of the different original reactants.

The simplest presumption for the energy redistribution at an interface is that the condensation energy is shared equally between the reactant and the solid products, which is expressed as $\tau=0.5$. The deviations, where Δ_cH° is distributed unequally between the solid reactant and the product phases in the ratio $\tau/(1-\tau)$, are ascribed to the degree of supersaturation of the non-volatile vapor.

The Arrhenius model is often represented by the familiar graph of energy variations as the reaction progresses by the "Advance along the Reaction Coordinate". This shows an initial rise to a maximum value, to form the 'transition complex', being followed by a decline thereafter. The activation energy is then the energy required for forming the 'activated' transition complex in an assumed "rate-determining step". However, in CDV theory, the value of parameter E represents the vaporization enthalpy [70].